

See discussions, stats, and author profiles for this publication at: <https://www.researchgate.net/publication/257022021>

# Finite element nonlinear dynamic analysis of sandwich plates with partially detached facesheet and core

ARTICLE in FINITE ELEMENTS IN ANALYSIS AND DESIGN · DECEMBER 2012

Impact Factor: 2.02 · DOI: 10.1016/j.finel.2012.08.003

---

CITATIONS

8

READS

43

## 2 AUTHORS:



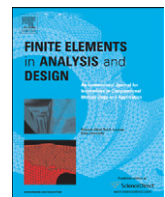
Vyacheslav N. Burlayenko  
Kharkiv Polytechnical Institute  
32 PUBLICATIONS 165 CITATIONS

[SEE PROFILE](#)



Tomasz Sadowski  
Lublin University of Technology  
179 PUBLICATIONS 1,203 CITATIONS

[SEE PROFILE](#)



## Finite element nonlinear dynamic analysis of sandwich plates with partially detached facesheet and core

V.N. Burlayenko <sup>a,b,\*</sup>, T. Sadowski <sup>a</sup>

<sup>a</sup> Department of Solid Mechanics, Lublin University of Technology, 40 Nadbystrzycka Street, 20-618 Lublin, Poland

<sup>b</sup> Department of Applied Mathematics, National Technical University 'KhPI', 21 Frunze Street, 61002 Kharkov, Ukraine

### ARTICLE INFO

#### Article history:

Received 28 December 2011

Received in revised form

9 August 2012

Accepted 9 August 2012

#### Keywords:

Sandwich plate

Nonlinear vibrations

Facesheet-to-core debonding

Finite element method

### ABSTRACT

A finite element model has been developed for analyzing of the dynamic response of sandwich plates with partially damaged facesheet-to-core interface. The effect of intermittent dynamic contact between the fragments detached at the damaged interface is taken into account for simulation of sandwich plates' vibrations. Transient and forced dynamic responses of the sandwich plates damaged by debonding have been obtained by using the ABAQUS/Explicit code. The influence of the local strongly nonlinear contact behavior on the global dynamics of the sandwich plates is examined.

© 2012 Elsevier B.V. All rights reserved.

### 1. Introduction

The finite element method (FEM), developed in recent few decades is most widely used for solving complex topological problems of physical fields and multi-field problems. Nonlinear finite element (FE) analyses are being now abundantly carried out. There are some FE formulations and algorithms which are well-established and known as accurate and reliable [1]. Such numerical concepts are implemented into various commercial and research FE codes as standard procedures. However, as a successful development of new materials and manufacturing processes is being reported, research problems become more complex and they have to be analyzed as a multistep task joining sequentially different subtasks. Consequently, although the standard procedures can be adopted for solving complex problems, the connection between analysis steps and the compatibility of the numerical procedures used in such steps are crucial in obtaining robust and efficient solution algorithms. These issues should be investigated and well-known in detail before performing of any analysis.

In this paper we consider, from the computational standpoint, the dynamics of a sandwich plate in which a penny-shaped segment of the facesheet is detached from the core in one of the interface layers. The analysis developed herein for the

numerical solution of the problem relies on a standard FE model and on an explicit FE method. Its peculiarity and novelty may be evaluated as follows: the efficiency of finite element solutions based on the combination of the used numerical procedures is demonstrated; the obtained results show real life simulations, which allow us to investigate better such phenomenon as nonlinear dynamics of the sandwich plate as well as provide potentially useful data in their practical relevance. In this respect, the vibration-based health monitoring technique is one of possible fields where these simulations would be implemented.

The engineering motivation of this study is provided primarily by using panels made of sandwich materials as basic structural components in aeronautical, aerospace and naval constructions. From the structural point of view sandwich panels possess much advantages over the conventional metallic counterparts, but they are very prone to damaging. One of the most common defects encountered in the sandwich panels is a partial separation between the facesheet and the core along their interface, called as facesheet-to-core debonding [2]. Because sandwich panels are often considered as vibrating structures, they should be designed so that to sustain in-service dynamic loads with the existing interfacial damage. The physical model of a vibrating sandwich panel is intrinsically nonlinear due to full coupling between vibrations, intermittent contact in detached segments and possible fracture at the boundary of the debonded zone. Hence, to analyze the complex dynamics of such panels, a nonlinear multi-step FE analysis has to be performed. In the present work we limit ourselves to nonlinear effects resulting from intermittent contact only, and the debonding growth problem is not considered.

\* Corresponding author at: Department of Applied Mathematics, National Technical University 'KhPI', 21 Frunze St., 61002 Kharkov, Ukraine.

E-mail addresses: burlayenko@yahoo.com (V.N. Burlayenko), t.sadowski@pollub.pl (T. Sadowski).

URL: <http://akropolis.pol.lublin.pl/users/sadowski/index.htm> (T. Sadowski).

Various attempts have been made by many researchers to describe in a unified manner the nonlinear free and forced vibrations of delaminated or debonded composite beams, plates and shells [3]. A considerable amount of previous theoretical works have been carried out for studying the modal characteristics of delaminated beams with an assumption that detached surfaces at the delaminated interface do not interact with each other during vibrations. Instead, researchers assumed that the surfaces either are freely vibrating in ‘free mode’ models [4,5] or are always closing in ‘constrained mode’ models [6–8]. Other authors, to avoid the interpenetration between the detached layers, inserted springs prescribing to them piecewise-linear properties, e.g. [9]. Studies of free vibrations of delaminated beams and plates using the FEM have been also broadly presented. For example, one-dimensional FE models were presented in [10,11]. More complex two-dimensional FE models were developed by applying either the first-order shear deformation theory as in [12] or the higher-order shear deformation theory as in [13] or the zig-zag theory as in [14] or the layerwise theory as in [15]. The modal analysis using three-dimensional plate models can be found, e.g. in [16] with the free mode formulation and in [17] with the spring element model.

In contrast to the aforementioned works, investigations of the dynamics of delaminated composite structures accounting for contact between detached segments are less presented in the literature. It is mainly because of the complexity of problem. One of the possibilities to tackle such complex task is the use of the analytical approach, replacing a continuous cracked structure with a single-DOF or multi-DOF oscillator. Those models were successful to reveal nonlinear response of composite beams with interfacial damage such as super- and subharmonics resonances and period doubling bifurcations, e.g. [18–20]. The influence of internal energy dissipation on the dynamic response of delaminated sandwich beams due to impact-like contact in the detached parts is discussed on the basis of discrete oscillator models within the framework of non-smooth dynamics in [21,22]. Another class of modeling techniques for studying nonlinear dynamics of composite structures damaged along structural interfaces uses order reduction methods based on nonlinear normal modes (NNM). In particular, the perturbation method and NNMs were used in [23] to study nonlinear vibrations of a delaminated beam. By using the proper orthogonal modes computed from nonlinear forced responses and their approximation by a truncated set of linear normal modes (LNM) with special boundary conditions, forced oscillations of a delaminated plate with the contact nonlinearity were modeled in [24].

Although the oscillator models, used in those studies have thrown a light on nonlinear phenomena of cracked structures they suffer from the lack of a spatial presentation of both deformation modes and distributions of interlaminar stresses. Thereby, continuum-based models of vibrating damaged structures, explicitly describing the interaction between detached segments are still highly required. Several analytical one-dimensional beam models for solving this problem have been proposed. A nonlinear constraint spring model of the delaminated interface of a composite beam was utilized in [25] for studying its free and forced oscillations. Authors in [26] have employed the Galerkin method and harmonic balance method to study nonlinear vibrations of composite beams with a through-width delamination. A high-order semi-analytical approach, based on the modified Galerkin method and the numerical implicit integration scheme was developed in [27] for studying free vibrations and a transient response of a simply supported debonded sandwich beam with a compressible core. Aforementioned models were able to capture the state of the delaminated interface in its two limit cases, either full closing or opening, but no interactions between the detached segments were possible to present.

In order to overcome the limitations of closed form solutions, dynamics of composite panels with contact has been studied using the FEM. FE modeling of such problems is not easy. It is well-known that if contact in a simulation has to be accounted for, many types of calculation difficulties occur, due to nonlinearity and non-smoothness of the associated equations. The implementation of FE procedures for contact analysis involves three principal aspects such as description of the contact interface geometry, enforcement of the contact conditions and treatment of the constraints imposed within a certain time integration scheme. The combination thereof is not straightforward and a number of different approaches have been proposed and researched. For more details in this item we refer to the classical books on contact mechanics, e.g. [28–30] as well as on new trends in this field in [31]. Some FE models, proposed for studying dynamics of composite panels accounting for contact at the damaged interface are reviewed below.

To describe intermittent contact between delaminated segments of a composite beam, the node-to-node frictionless contact formulation involving small deformation assumptions within the FE approach was used in [32]. The contact constraints were imposed by a modified Lagrange multiplier method. The Newmark iterative algorithm was exploited for solving the dynamic contact problem. Based on these numerical procedures dynamic responses of a delaminated beam subjected to both impulse and harmonic loads were simulated. Authors in [33,34] have investigated the dynamic response of delaminated beams and a debonded sandwich plate, respectively, using 2-D FE models in conjunction with kinematic constraints governing contact–impact conditions at the damaged interfaces. The node-to-node contact constraints, imposed via the penalty method in the vibration problem of a laminated plate were utilized in [35]. The transient analysis of delaminated composite and smart composite plates was studied in [36] using an improved layerwise laminate theory, extended to include large deformation and the interlaminar contact during ‘breathing’ phenomena in the delaminated zone. The breathing phenomenon was described using two different contact spring models and the associated equations were integrated by using the Newmark-beta implicit algorithm with Newton–Raphson iteration, modified to be a predictor–corrector method. A FE model of a composite plate with multiple delaminations based on the higher-order zig-zag plate theory was developed in [37] for the dynamic analysis. The Lagrange multiplier method to impose the unilateral contact conditions within delaminated interfaces was applied in that work. A further contribution into a nonlinear dynamic behavior of sandwich plates with interfacial damage can be found in [38], where a sandwich plate containing a post-impact zone was modeled by a three-dimensional FE model within the ABAQUS code. Recent progress in FE methodologies in the form of the extended finite element method (XFEM) have been adopted for evolving dynamic problems of cracked plates, e.g. in [39,40] as well as crack growth problems with contact, e.g. in [41–43]. Researches regarding enforcements of contact constraints at a discontinuity interface within the framework of the XFEM are done in [44]. It should be noticed that the XFEM have already become a standard algorithm for the crack propagation analysis in several commercial FE codes, e.g. [45].

The literature search showed that still a few three-dimensional simulations of delaminated plates have been done, if there is something similar, it is not taking into account the problem of intermittent contact. Thus, the aim of this paper is to investigate a dynamic behavior of sandwich plates with partially detached facesheet-to-core interface by finite element simulations. We intend to develop a model of a debonded sandwich plate, which captures the dominant nonlinearities arising from the local

contact phenomenon within the debonded zone, and to show their influences on the global dynamics of the plate. Pursuing this objective, to develop an appropriate computational model we first formulate the weak form of the elastodynamic contact problem involving non-smooth Signorini's and Coulomb's contact laws in the usual formalism of continuum mechanics. Second, we make a finite element discretization of the dynamic contact problem within the explicit time-stepping scheme. Finally, on the basis of these underlying concepts the finite element model of the debonded sandwich plate with a penny-shaped detached region is developed using the general purpose FE code ABAQUS/Explicit, where finite elements and numerical procedures available in the code are used in simulations. Both a transient response and a behavior under periodic loading of the sandwich plate are simulated and results are discussed in detail.

## 2. Statement of the problem

For the sake of completeness, the mathematical aspects of the general elastodynamic problem of a continuum with a discontinuity, whose surfaces are able to interact with each other, are briefly discussed in this section. In order to focus only on nonlinear effects arising from dynamic contact, the simplest case involving linear elasticity and small strains is considered. We follow the works [28–30], to which we refer for more details in this problem. Throughout this work we adopt the notations which are usual in most of the books on continuum mechanics, e.g. [46].

### 2.1. Variational equality formulation

First a variational formulation of the problem under consideration is presented. Let us consider a deformable body occupying a domain  $\Omega \in \mathcal{R}^3$  at time  $t \in [0, T]$  and  $\Gamma \in \mathcal{R}^2$  is its boundary such that  $\Gamma_t \cup \Gamma_u = \Gamma$  and  $\Gamma_t \cap \Gamma_u = \emptyset$ , as shown in Fig. 1a. Herein  $\Gamma_t$  and  $\Gamma_u$  stand for the boundaries with prescribed tractions  $\bar{\mathbf{t}}$  and displacements  $\bar{\mathbf{u}}$ , respectively. We allow this domain to contain an internal discontinuity, described by a surface  $\Gamma_c$ . Let  $\tilde{\Omega}$  be the open set, which excludes all discontinuities, i.e.  $\tilde{\Omega} = \Omega \setminus \Gamma_c$ .

From a mathematical point of view, any problems involving contact should be rigorously solved by using methods of variational inequalities [47–49]. Such approaches, however, are not directly applicable for implementation in FE analyses. In practice of the FEM, the active set method is used whereby the variational formulation can be extended to the treatment of contact problems, e.g. [29,30]. Following this approach the contact surface  $\Gamma_c$  and, consequently, an active set of constraints are presumed to be known within an incremental solution step. Hence, contact forces along with displacements are primary unknowns which can be found in the specific instant of time. There are many strategies for incorporating the active set concept in conjunction with calculations of the contact forces into FE algorithms, in particular, the penalty method, the augmented Lagrangian technique, the

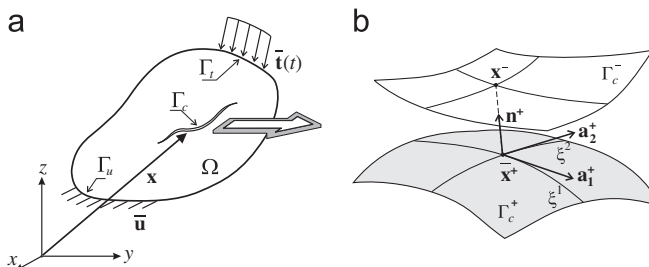


**Fig. 1.** A body with a discontinuity: (a) representation of the body in the reference and the current domains and (b) zoom of the discontinuity's surfaces.

perturbed Lagrangian method, a form of barrier method, etc. [29,30]. In the present work, the kinematic contact algorithm is used for imposing contact constraints.

The principle of virtual work can provide the variational formulation of the elastodynamic problem of the body with taking into account contact between the crack faces as follows [1,29]: for every time  $t \in [0, T]$  find  $\mathbf{u}(t) \in U$  such that

$$\begin{aligned} & \int_{\tilde{\Omega}} \delta \mathbf{u} \cdot \rho \ddot{\mathbf{u}} d\Omega + \int_{\tilde{\Omega}} \delta \mathbf{u} \cdot c \dot{\mathbf{u}} d\Omega + \int_{\tilde{\Omega}} \delta \boldsymbol{\varepsilon} : \boldsymbol{\sigma} d\Omega \\ &= \int_{\tilde{\Omega}} \delta \mathbf{u} \cdot \rho \mathbf{b} d\Omega + \int_{\Gamma_t} \delta \mathbf{u} \cdot \bar{\mathbf{t}} d\Gamma + \delta W^c, \quad \forall \delta \mathbf{u} \in U_0 \end{aligned} \quad (1)$$

with given boundary conditions  $\boldsymbol{\sigma} \cdot \mathbf{n} = \bar{\mathbf{t}}$  on  $\Gamma_t$  and  $\mathbf{u} = \bar{\mathbf{u}}$  on  $\Gamma_u$  and contact interface conditions on  $\Gamma_c$ , and initial conditions  $\mathbf{u}(0) = \mathbf{u}_0$  and  $\dot{\mathbf{u}}(0) = \mathbf{v}(0) = \mathbf{v}_0$  in  $\tilde{\Omega}$ . Herein the trial solutions  $\mathbf{u}(t)$  and the test functions  $\delta \mathbf{u}$  reside in appropriate vector spaces for the displacement fields defined as follows:

$$U = \{\mathbf{u} \mid \mathbf{u} \in \mathcal{H}^1(\tilde{\Omega}), \mathbf{u} = \bar{\mathbf{u}} \text{ on } \Gamma_u, \text{ discontinuous on } \Gamma_c\} \quad (2)$$

$$U_0 = \{\delta \mathbf{u} \mid \delta \mathbf{u} \in \mathcal{H}^1(\tilde{\Omega}), \delta \mathbf{u} = 0 \text{ on } \Gamma_u \cup \Gamma_c\} \quad (3)$$

In Eq. (1) we stand for that  $\rho$  is the mass density,  $c$  is the linear viscous damping parameter which represents the system material damping,  $\mathbf{b}$  are the body forces,  $\mathbf{n}$  is the outward unit normal to  $\Omega$ ,  $\mathbf{u}$  are the displacements, and  $\boldsymbol{\sigma}$  and  $\boldsymbol{\varepsilon}$  denote the Cauchy stress tensor and the infinitesimal strain tensor  $\boldsymbol{\varepsilon} = \frac{1}{2}(\nabla \mathbf{u} + (\nabla \mathbf{u})^T)$ , respectively, which are related by the linear elastic constitutive model  $\boldsymbol{\sigma} = C : \boldsymbol{\varepsilon}$  with the fourth-order stiffness tensor  $C$ .

It follows from (1) that the total energy in the body with crack contains two parts, where the first part comprises the terms widely recognized such as inertial, damping, internal and external works, and the second one comes from contribution of a contact traction  $\mathbf{t}_c = \boldsymbol{\sigma} \cdot \mathbf{n}_c$  at contact points of the discontinuity  $\Gamma_c$ , where  $\mathbf{n}_c$  is the outward unit normal at these points. With this at hand, the virtual work equation (1) can be recast into such form that each of the terms will reflect its physical meaning mentioned above. Thereby, in the order of declaration of the quantities we can write down the algebraic sum of the virtual works as follows:

$$\delta W^{inert} + \delta W^{damp} + \delta W^{int} - \delta W^{ext} - \delta W^c(\mathbf{t}_c) = 0 \quad (4)$$

As mentioned above, the contact virtual work in (4) is only contributed to by points  $\mathbf{x} \in \Gamma_c$  where contact constraints are active. A general form of this term at the instant of time when contact is active can be defined by the expression

$$\delta W^c = \int_{\Gamma_c} (t_N \delta g_N + \mathbf{t}_T \cdot \delta \mathbf{g}_T) d\Gamma \quad (5)$$

Here, in terms of the 'master-slave' approach used usually in FE contact formulations,  $g_N = (\mathbf{x}^- - \bar{\mathbf{x}}^+) \cdot \bar{\mathbf{n}}^+$  is a gap function defining a minimal distance between a node of the slave surface  $\mathbf{x}^- \in \Gamma_c^-$  and its orthogonal projection on the master surface  $\bar{\mathbf{x}}^+(\xi^1, \xi^2) \in \Gamma_c^+$  with the unit normal  $\bar{\mathbf{n}}^+$ , where  $\xi^\alpha$  with  $\alpha = 1, 2$  denotes the parametrization of the surface (see Fig. 1b).

Analogously,  $\mathbf{g}_T$  stands for a tangential gap function describing a relative tangential movement of the surfaces with respect to each other and associated with a friction phenomenon. This vector-function can be defined by  $\mathbf{g}_T = g_{T_\alpha} \bar{\mathbf{a}}_\alpha^+$  with  $g_{T_\alpha} = (\mathbf{x}^- - \bar{\mathbf{x}}^+) \cdot \bar{\mathbf{a}}_\alpha^+$ , where  $\bar{\mathbf{a}}_\alpha$  with  $\alpha = 1, 2$  are tangent base vectors at the point  $\bar{\mathbf{x}}^+$  (see Fig. 1b) such that  $\bar{\mathbf{n}}^+ = \bar{\mathbf{a}}_1^+ \times \bar{\mathbf{a}}_2^+ / \| \bar{\mathbf{a}}_1^+ \times \bar{\mathbf{a}}_2^+ \|$ .

In the tangential direction, one needs to differ between sticking and sliding states on the contact surfaces [50]. As long as sticking takes place, no tangent sliding between contact surfaces occurs, consequently, no difference between the normal and tangent behavior, i.e. the gap function vanishes,  $\dot{\mathbf{g}}_T = 0 \Leftrightarrow \mathbf{g}_T = 0$ . Otherwise, the contacting surfaces slide with respect to each other fulfilling impenetrability condition exactly

$(g_N = 0)$ . In this case the projection point moves on the master surface by forming a path which is not known *a priori*. Hence in a frictional sliding situation, one has to integrate the relative tangential velocities to obtain the path of  $\bar{\mathbf{x}}^+$  on the master surface. In the geometrically linear case, the rate of tangential gap function at the contact point can be found as  $\dot{\mathbf{g}}_T = \dot{\xi} \bar{\mathbf{a}}_\alpha^+ = \dot{g}_{T_\alpha} \bar{\mathbf{a}}_\alpha^+$  with  $\dot{g}_{T_\alpha} = (\mathbf{x}^- - \bar{\mathbf{x}}^+) \cdot \bar{\mathbf{a}}_\alpha^+ = a_{\alpha\beta} \dot{\xi}$ , where  $a_{\alpha\beta} = \bar{\mathbf{a}}_\alpha^+ \cdot \bar{\mathbf{a}}_\beta^+$  is the metric tensor at  $\bar{\mathbf{x}}^+$  on  $\Gamma_c^+$ .

The contact traction  $\mathbf{t}_c$  at the contact point  $\bar{\mathbf{x}}^+$  is decomposed into normal and tangential components, i.e.  $\mathbf{t}_c = \mathbf{t}_N + \mathbf{t}_T$ , where  $\mathbf{t}_N = t_N \bar{\mathbf{n}}^+$  and  $\mathbf{t}_T = t_{T_\alpha} \bar{\mathbf{a}}_\alpha^+$  with  $\alpha = 1, 2$ . The scalars  $t_N$  and  $t_{T_\alpha}$  represent the normal and tangential quantities of the contact pressure, respectively. Herewith, the normal traction (a compressive force) always points inward and the tangent traction (the frictional force) opposes to the relative sliding direction. Moreover, at the contact point the interior continuity conditions on the stresses should be met accordingly with Newton's third law as  $\sigma^+ \cdot \mathbf{n}^+ = -\sigma^- \cdot \mathbf{n}^- = \mathbf{t}_c$ .

With notations introduced we formulate the normal contact conditions enforcing the physical requirements of impenetrability and compressive character of interactions, as shown in Fig. 2a, in the following form:

$$t_N \leq 0, \quad g_N \geq 0 \quad \text{and} \quad t_N g_N = 0, \quad (6)$$

which are known as Karush–Kuhn–Tucker conditions.

The contact conditions in tangential directions associated with the frictional behavior can also be given in the form of inequalities as follows [50]:

$$\|\mathbf{t}_T\| \leq \tau_{crit}, \quad \|\mathbf{g}_T\| \geq 0, \quad (\|\mathbf{t}_T\| - \tau_{crit}) \|\mathbf{g}_T\| = 0 \quad (7)$$

where  $\tau_{crit}$  is a threshold of tangential contact traction for tangential slip, Fig. 2b. If the frictional model is characterized by Coulomb's law, we have  $\tau_{crit} = \mu t_N$ , where  $\mu$  is the coefficient of friction.

Because of the analogy between the friction phenomenon and plasticity, the plasticity framework has often been used to Coulomb's friction law [29,30]. In this case the total tangential gap  $\mathbf{g}_T$  is split into an 'elastic' stick part and a 'plastic' slip part  $\mathbf{g}_T = \mathbf{g}_T^{stick} + \mathbf{g}_T^{slip}$ . For sticking an elastic constitutive relation  $\mathbf{t}_T = \epsilon_T \mathbf{g}_T^{stick}$  is applied, where  $\epsilon_T$  denotes the penalty parameter. The regularization of Coulomb's friction law is portrayed by the dotted line in Fig. 2b. An evolution law for the slip part is based on a slip potential function taking the form  $\Phi(\mathbf{t}_T) = \|\mathbf{t}_T\| - \mu t_N$ . Finally, for slipping we have

$$\dot{\mathbf{g}}_T^{slip} = \dot{\gamma} \frac{\partial \Phi(\mathbf{t}_T)}{\partial \mathbf{t}_T} = \dot{\gamma} \frac{\mathbf{t}_T}{\|\mathbf{t}_T\|} \quad (8)$$

along with loading–unloading conditions in Kuhn–Tucker form

$$\Phi \leq 0, \quad \dot{\gamma} \geq 0 \quad \text{and} \quad \Phi \dot{\gamma} = 0 \quad (9)$$

In the case  $\Phi > 0$  the sticking takes place.

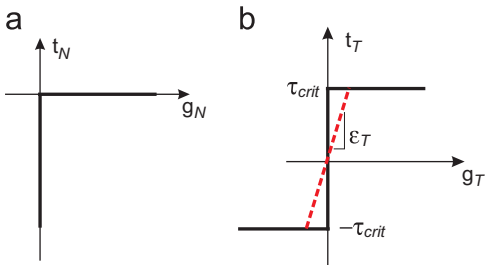


Fig. 2. (a) Normal contact conditions and (b) tangential contact conditions.

## 2.2. Finite element formulation

Following the FE approach, the variational equation (1) should be discretized. Let the current domain  $\Omega$  be subdivided into a number of element subdomains  $\Omega_e$  so that the union of the elements comprises the total discretized domain  $\Omega^h = \bigcup_e \Omega_e$  and the domain  $\Omega$  is replaced by  $\Omega^h$ . Due to the concept of a finite-dimensional approximation of a space, the finite-dimensional vector spaces  $U^h$  and  $U_0^h$  can be defined as subsets of the corresponding infinite counterparts, i.e.  $U^h \subset U$  and  $U_0^h \subset U_0$ , respectively. Then, approximate displacement fields  $\mathbf{u}^h(t)$  and their variations  $\delta\mathbf{u}^h$  within each finite element are functions pertaining to these finite-dimensional spaces and can be expressed in terms of nodal values as follows:

$$\mathbf{u}^h(t) = \mathbf{u}_I(t) N_I \quad \text{and} \quad \delta\mathbf{u}^h = \delta\mathbf{u}_I N_I, \quad (10)$$

where  $N_I$  are the shape functions associated with the  $I$ th node,  $\mathbf{u}_I(t)$  and  $\delta\mathbf{u}_I$  are the nodal quantities at node  $I$ . Summation over repeated indices is implied. It should be recalled that in the spatial discretization of the displacements in (10) their temporal continuity at nodes is maintained. The velocities and accelerations can be found as the material derivatives of the displacements,

$$\mathbf{v}^h(t) = \dot{\mathbf{u}}^h(t) = \dot{\mathbf{u}}_I(t) N_I \quad \text{and} \quad \ddot{\mathbf{u}}^h(t) = \ddot{\mathbf{u}}_I(t) N_I \quad (11)$$

Substituting of these finite dimensional quantities into the variational principle (1), an approximate FE solution of the problem stated above in the continuum form can be formulated as follows: for given the boundary conditions  $\bar{\mathbf{t}}$  on  $\Gamma_t^h$ ,  $\bar{\mathbf{u}}$  on  $\Gamma_u^h$ , the initial conditions  $\mathbf{u}_0$  and  $\mathbf{v}_0$  in  $\bar{\Omega}^h$ , the distributed body forces  $\mathbf{b}$  in  $\bar{\Omega}^h$  and the contact conditions on  $\Gamma_c^h$  find  $\mathbf{u}^h(t) \in U^h$  for every time  $t \in [0, T]$  such that

$$\begin{aligned} & \int_{\bar{\Omega}^h} \delta\mathbf{u}^h \cdot \rho \ddot{\mathbf{u}}^h d\Omega + \int_{\bar{\Omega}^h} \delta\mathbf{u}^h \cdot c \dot{\mathbf{u}}^h d\Omega + \int_{\bar{\Omega}^h} \delta\mathbf{e}^h : \boldsymbol{\sigma}^h d\Omega \\ &= \int_{\bar{\Omega}^h} \delta\mathbf{u}^h \cdot \rho \mathbf{b} d\Omega + \int_{\Gamma_t^h} \delta\mathbf{u}^h \cdot \bar{\mathbf{t}} d\Gamma + \int_{\Gamma_c^h} (t_N^h \delta g_N^h + \mathbf{t}_T^h \cdot \delta \mathbf{g}_T^h) d\Gamma, \end{aligned} \quad (12)$$

for all admissible  $\delta\mathbf{u}^h \in U_0^h$ . All quantities in (12) are finite-dimensional counterparts of those given for the continuous case in (1). In particular,  $\boldsymbol{\sigma}^h$  refers to the stress field obtained by substitution of the approximate solution  $\mathbf{u}^h$  into Hooke's law and the virtual strain field  $\delta\mathbf{e}^h$  by substitution of the variation of the approximate solution  $\delta\mathbf{u}^h$  into the small strain-displacement relationships. The integrand of the contact integral deserves special consideration since its discretization is not trivial. First, the components of contact traction  $t_N^h$  and  $\mathbf{t}_T^h$ , related via the constraint conditions (6) and (7) to  $g_N^h$  and  $\mathbf{g}_T^h$  on the discretized surface  $\Gamma_c^h$ , have definitions that depend upon the solution method utilized. Consequently, their explicit descriptions are deferred until the solution algorithm applied is presented. In turn, the kinematic variables  $\delta g_N^h$  and  $\delta \mathbf{g}_T^h$ , which are functions of the approximate solution  $\mathbf{u}^h$ , are calculated depending on the discretization approach used on  $\Gamma_c^h$ . One of the approaches either node-to-node or node-to-surface or surface-to-surface should be chosen. Finally, before any contact model can be utilized the contact surface  $\Gamma_c^h$  must firstly be identified. The active constraint set is located by the iterative process called as contact detection (searching). Briefly this algorithm involves the following two phases: the first search (global) locates segments that are close to each other, whereas the second one (local) is applied to the segments being found for calculating the discrete gap functions  $g_N^h$  and  $\mathbf{g}_T^h$  on  $\Gamma_c^h$  being known.

Using the definitions of the physical names to each of the terms in (12) given by (4), the set of finite element equations of

motion via the corresponding nodal forces takes the form

$$\mathbf{M}\ddot{\mathbf{U}}(t) + \mathbf{C}\dot{\mathbf{U}}(t) + \mathbf{K}\mathbf{U}(t) = \mathbf{F}^{ext}(\mathbf{U}(t)) - \mathbf{F}^{cont}(\mathbf{U}(t)) \quad (13)$$

In (13)  $\ddot{\mathbf{U}}(t)$ ,  $\dot{\mathbf{U}}(t)$  and  $\mathbf{U}(t)$  are the global vectors of unknown accelerations, velocities and displacements,  $\mathbf{F}^{ext}$  and  $\mathbf{F}^{cont}$  are the global vectors of external and contact forces resulting from the definitions of virtual external and contact works in (4), and  $\mathbf{M}$ ,  $\mathbf{C}$  and  $\mathbf{K}$  are the global mass, damping and stiffness matrices derived by manipulations with the virtual inertial, damping and internal works in the same expression. These global vectors and matrices are typically calculated as an assembly of element level contributions.

As shown by many investigations in the field of dynamics, it is difficult to derive explicit expressions related to dissipation of the vibrating energy in a structure. Instead, simplified models, based rather on mathematical convenience than physical representation, are used which, in many cases, have been found to be adequate [51]. The most common form of viscous damping, associated with system material damping is the Rayleigh-type, when damping forces are proportional to the velocities of oscillation via the following damping matrix:

$$\mathbf{C} = \alpha\mathbf{M} + \beta\mathbf{K} \quad (14)$$

The factors  $\alpha$  and  $\beta$  can be determined on the basis of the modal damping ratio:

$$\xi_n = \frac{\alpha}{2\omega_n} + \frac{\beta\omega_n}{2} \quad (15)$$

by specifying any desirable ratio for any two selected frequencies  $\omega_n$  of the undamped system with the given  $\mathbf{M}$  and  $\mathbf{K}$ .

Thus, the motion at any time is fully defined by (13) and by initial conditions on  $\mathbf{U}(t)$  and  $\dot{\mathbf{U}}(t)$ . In (13) we have presented the spatially discretized form of the problem with the time dimension kept continuous. Next a time-stepping procedure to complete a total discretization has to be applied. For this the time interval  $[0, T]$  is divided into non-overlapping subintervals such that  $[0, T] = \bigcup_{i=0}^{L-1} [t_i, t_{i+1}]$ , where  $t_i < t_{i+1}$ , and  $t_0 = 0$ ,  $t_L = T$ . Hence, the solution satisfying (13) can only be found in a finite number of time steps. Let the time increment be  $\Delta t_{i+1} = t_{i+1} - t_i$  and for the simplicity accelerations, velocities and displacements referring to this time increment are denoted by  $\ddot{\mathbf{U}}_{i+1}$ ,  $\dot{\mathbf{U}}_{i+1}$  and  $\mathbf{U}_{i+1}$ , respectively. Then the totally discretized dynamic equilibrium equation at a certain time  $t_{i+1} = t_i + \Delta t_{i+1}$  reads as follows:

$$\mathbf{M}\ddot{\mathbf{U}}_{i+1} + \mathbf{C}\dot{\mathbf{U}}_{i+1} + \mathbf{K}\mathbf{U}_{i+1} = \mathbf{F}_{i+1}^{ext} - \mathbf{F}_{i+1}^{cont}$$

with given  $\mathbf{U}_0 = \bar{\mathbf{U}}$  and  $\dot{\mathbf{U}}_0 = \bar{\mathbf{V}}$  (16)

There are a wide range of time-stepping algorithms that have been employed for solving the incremental problem posed by the equation-type (16). These algorithms can commonly be categorized into two schemes: implicit methods and explicit methods. In an implicit time-stepping scheme at each time increment a system of simultaneous equations has to be solved iteratively to find an approximate equilibrium state at this increment. Thus, it is a combination of incremental and iterative procedures. Such schemes work independently of a time increment size and are thus unconditionally stable [1]. But due to solving the system of simultaneous equations at each iteration implicit methods require significant computational efforts in particular for strongly nonlinear dynamic problems.

Unlike the implicit schemes, explicit time-stepping algorithms determine the solution of equations like (16) without iterations and tangent stiffness matrix by explicit advancing of the kinematic state known from a previous increment to the next one. To introduce the concept of the explicit algorithm, the central-difference formulation can be exploited [1,46]. First, accelerations at the beginning of each increment  $\Delta t_{i+1}$  are calculated by using

Eq. (16) reexpressed in the form

$$\ddot{\mathbf{U}}_i = \mathbf{M}^{-1}(\mathbf{F}_i^{ext} - \mathbf{F}_i), \quad (17)$$

where  $\mathbf{F}_i^{ext}$  is the vector of the given external nodal forces at time  $t_i$  and  $\mathbf{F}_i$  is the sum of nodal internal  $\mathbf{F}_i^{int} = \mathbf{K}\mathbf{U}_i$ , damping  $\mathbf{F}_i^{damp} = \mathbf{C}\dot{\mathbf{U}}_i$  and contact  $\mathbf{F}_i^{cont}$  forces which are updated during the previous time increment  $\Delta t_i$ . Thereafter, the central difference operator uses the accelerations calculated at  $t_i$  to advance the velocity solution to time  $t_i + \frac{1}{2}\Delta t_{i+1}$  and the displacement solution to time  $t_i + \Delta t_{i+1}$  as follows:

$$\begin{aligned} \dot{\mathbf{U}}_{i+1/2} &= \dot{\mathbf{U}}_{i-1/2} + \frac{\Delta t_{i+1} + \Delta t_i}{2} \ddot{\mathbf{U}}_i \\ \mathbf{U}_{i+1} &= \mathbf{U}_i + \Delta t_{i+1} \dot{\mathbf{U}}_{i+1/2} \end{aligned} \quad (18)$$

The initial half-step lagging velocity ( $\dot{\mathbf{U}}_{-1/2}$ ) is calculated from the initial velocity assuming the initial acceleration to have been constant over the lagging half-step.

The key to the computational efficiency of the explicit procedure is the use of diagonal element mass matrices because the inversion of the mass matrix that is used in the computation for the accelerations in (17). Thus, using the explicit time integration to solve (16) the lumped mass matrix  $\mathbf{M}$  is used. The procedures for reducing the consistent mass matrix to its diagonal form are well-known, e.g. [1,46]. Because the accelerations of any node is completely defined by its mass and the nodal forces, there are no equations to be solved simultaneously. Thus the explicit scheme is less computationally expensive for each time increment than the implicit one. Moreover, the computational cost for the explicit method is approximately proportional to the size of a FE model and does not change as dramatically as for implicit methods.

The disadvantage of the explicit procedure is that the time increment used in an analysis must be smaller than the stability limit of the central-difference operator. An estimation of this limit is the transit time of a dilatational wave ( $c_d$ ) across the length of the smallest element in a FE mesh ( $L_e$ ):

$$\Delta t_{crit} \approx \frac{L_e}{c_d} \quad (19)$$

### 3. Finite element modeling

The FE approach, described in the previous section to model a nonlinear dynamic behavior accounting for contact conditions is being applied for simulating dynamics of a sandwich plate containing a penny-shaped zone detached between the core-to-facesheet interface. The simulations are carried out with the ABAQUS/Explicit code [45]. The finite element model of the sandwich plate is shown in Fig. 3a. It takes the sandwich plate modeling idea of [53], where the facesheets are represented as Reissner–Mindlin plates whereas the core is modeled as a three-dimensional continuum. That modeling capability enables to give accurate results at less computational cost, compared with a fully three-dimensional model, for analyzing a broad range of sandwich plate problems. Especially whenever the sandwich core is flexible and localized effects such as intermittent contact between detached segments occur.

Since the facesheets refer to structures in which one dimension, the thickness, is significantly smaller than the other dimensions, structural shell finite elements are used to model them. In this respect either conventional or continuum shell elements are possible. The conventional shell elements discretize a body by defining the geometry at a reference surface. In this case the thickness is defined through the section property definition. In contrast, the continuum shell elements discretize an entire three-dimensional body. The thickness is determined from the element

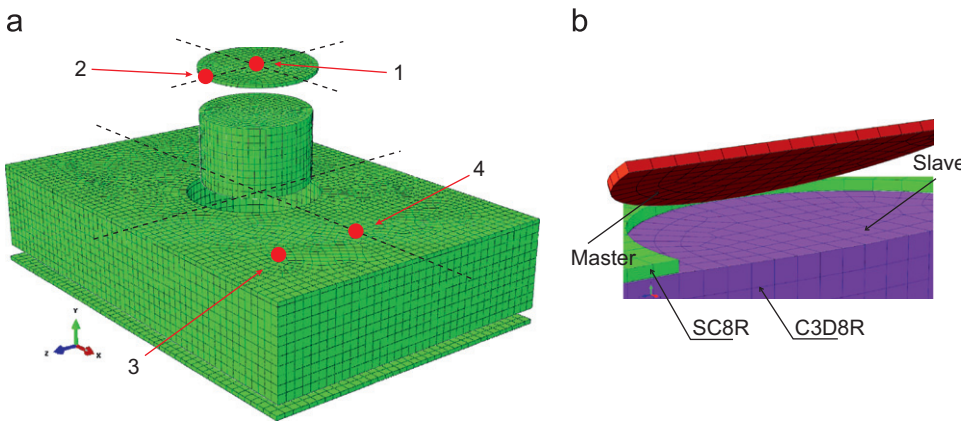


**Fig. 3.** (a) Three-dimensional FE model of the sandwich plate with penny-shaped debonding and (b) details of modeling at the debonding zone.

nodal geometry. From a modeling point of view the continuum shell elements look like three-dimensional continuum solids, but their kinematic and constitutive behavior is similar to the conventional shell elements. The reduced-integration 8-node continuum shell finite elements, SC8R are utilized in the current work. These elements are linear with translational degrees of freedom only. They are related to general-purpose elements that can provide solutions to both thin and thick shell problems. It means that the hypotheses of Reissner–Mindlin's shell theory are assigned to the elements kinematics as the shell thickness increases, and Kirchhoff's assumptions are fulfilled within the elements as the thickness decreases. In the case of laminated facesheets, the continuum shell elements can be stacked to recover a more refined through-the-thickness response of transverse shear stresses and forces. Moreover, the elements allow two-sided contact with changes in the thickness that is a useful capacity for the contact modeling [45].

The continuum shell elements can be directly connected to first-order continuum solids without any kinematic transition. On the other hand the Explicit code is limited by using the first-order brick elements only. Thus, 8-node isoparametric linear reduced-integration solid 'brick' elements C3D8R are exploited for discretizing the core. These elements have the advantage of alleviating difficulties of shear-locking inherent in fully integrated linear elements when bending loads are applied. However, they tend to suffer from hourglass modes under bending. Existence of these modes may lead to severe mesh distortion, with no stresses resisting the deformation. To minimize this problem, a hourglass control is introduced into these elements. The artificial stiffness method available by default in ABAQUS is used to calculate the hourglass-resisting forces. Moreover, in order to get the best results in an efficient manner, the improved 'Centroidal Strain' formulation to compute strains at the elements is utilized in simulations. Due to good performance and versatility these brick elements (C3D8R) can be used in models from simple linear analyses to complex nonlinear ones involving contact also. For more detailed information concerning element technology one can refer to [45].

The general three-dimensional FE mesh is generated by partition of the total model onto several parts, which are connected with each other through share nodes, Fig. 3a. The continuum shell elements are positioned on the upper and lower core sides and directly connected to the core. The penny-shaped debonded zone is presented by an actual small gap between the finite elements of the facesheet and core at the center of plate. The mesh density of the FE model is higher in portions, where the debonded zone is introduced and it decreases gradually from the penny-shaped debonded zone to the edges of plate. In doing so, the

discretization of the surfaces of the facesheet and core coming in contact at the debonded interface is performed with non-conforming but approximately equal mesh densities. No artificial adjustment of either the material or geometrical properties is made at the non-bonded region to ensure as close as possible a physically real case.

The surface-to-surface contact approach is used for discretizing the contacting surfaces between the facesheet and the core at the damaged interface. Due to this a planar approximation of the master surface per averaging region of the slave surface is performed. Thereby, the approach can handle non-matching grids. Since the surfaces coming into contact have high dissimilar mechanical properties, a pure master-slave contact pair formulation in ABAQUS/Explicit is used, Fig. 3b. Assuming small oscillations of the plates being studied, we accept a small-sliding displacement kinematics for describing the motion of the interacting surfaces with respect to each other. In the small-sliding formulation for an active contact pair every slave node interacts with its own local tangent plane on the master surface. Hence, ABAQUS does not have to monitor slave nodes for possible contact along the entire master surface [45]. Therefore, small-sliding contact is less expensive computationally than finite-sliding contact. The cost savings are most dramatic in three-dimensional contact problems.

The contact behavior of the surfaces interacting with each other in the normal direction is accepted to be governed by the 'hard contact' model, as shown in Fig. 2a. The model implies that in contact the surfaces transmit no contact pressure unless the nodes of the slave surface contact the master surface and no penetration is allowed at each constraint location. While the contact behavior in the tangential directions is given by the isotropic Coulomb friction model, Fig. 2b. The penalty parameter  $\epsilon_T$  is computed by ABAQUS automatically so that to satisfy some portion of a reversible tangential motion specified by a user and in order its effect on the time increment was minimal.

The kinematic contact algorithm available in ABAQUS/Explicit is used to enforce the contact constraints defined by (6) and (8) and (9). It is a predictor/corrector method enabling to impose exactly the constraints on the global equations by modifying the accelerations, velocities and displacements of nodes, at which contact is active in the current time increment. The method is based on the algorithm developed in [52] to which we refer for more details. The calculation of contact forces imposed on a master surface by a slave node within this algorithm can briefly be presented as follows:

- *predictor phase:* A kinematic state at the beginning of the increment  $\Delta t$  is calculated without regard to the constraints

required by the contact surfaces. For each node  $I$  the predicted acceleration can be found as

$$\ddot{\mathbf{U}}_I^{\text{pred}} = m_I^{-1} \mathbf{R}_I$$

where  $\mathbf{R}_I$  is the residual nodal force without a nodal contact force  $\mathbf{F}_I^{\text{cont}}$ ,  $m_I$  is the nodal mass. Then, predicted velocities and displacements for each node  $I$  are updated.

The predicted configuration can result in penetration, as shown by the configuration of a slave node in Fig. 4. Each node contacting with or penetrating through the master surface is included into a set of active contact,  $\mathcal{A}$ . For a slave node  $S$  from this set, the contact force resisting to penetration in the direction  $\mathbf{n}$  is calculated by using the penetration depth of the slave node  $d^{\text{pred}} = d(g_N^h)$ , its mass  $m_S$  and the time increment:

$$f_{N_S}^{\text{cont}} = \frac{m_S d^{\text{pred}}}{(\Delta t)^2}$$

- **corrector phase:** The corrected acceleration of each node  $S \in \mathcal{A}$  is calculated as

$$\ddot{\mathbf{U}}_S^{\text{corr}} = \ddot{\mathbf{U}}_S^{\text{pred}} + \ddot{\mathbf{U}}_{N_S}$$

where  $\ddot{\mathbf{U}}_{N_S}$  is an acceleration correction reflecting the response of the master surface to the corresponding contact forces  $f_{N_S}^{\text{cont}}$ . In this way, the vector of normal contact forces  $\mathbf{F}_{N_{i+1}}^{\text{cont}}$  is computed in the current time step.

The corrected accelerations are used to update the velocities and displacements to a final configuration in the current increment in which each slave node is exactly in compliance with the master surface, Fig. 4.

As it can be seen that the kinematic algorithm is essentially implicit, i.e. it seeks to eliminate the contact penetration at the end of each time increment. Due to this the kinematic algorithm has no effect on the ongoing calculation of the stable time increment during the analysis. It is unlike the penalty algorithm, which may have the effect of reducing the stable time increment, since the penalty springs increase the overall stiffness acting on the interface nodes.

For nodes which remain in contact in the increment  $\Delta t$  the tangential forces have to be evaluated according to Coulomb's frictional model. To include the friction into the algorithm mentioned above the following steps should additionally be done:

- in the predictor phase, after the update of the kinematic state to the predicted configuration the relative tangential velocity of each slave node  $S \in \mathcal{A}$  with respect to the master surface is calculated. Let its magnitude be defined by  $v^{\text{pred}} = v(g_{T_z})$ . Then, a predicted tangential force that will cancel the velocity tangential to the master surface in direction  $\mathbf{a}_x$  is computed as

$$f_{T_S}^{\text{pred}} = -\frac{m_S v^{\text{pred}}}{\Delta t}$$

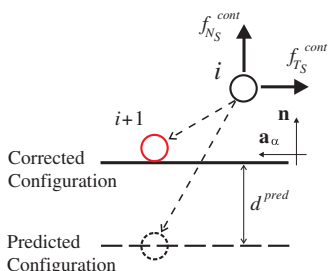


Fig. 4. Kinematic contact constraint algorithm.

Therefore the slip potential function (9) is defined by

$$\Phi^{\text{pred}} = f_{T_S}^{\text{pred}} - \mu f_{N_S}^{\text{cont}}$$

- in the corrector phase the tangential contact force is calculated depending on the slip potential as follows:

$$f_{T_S}^{\text{corr}} = f_{T_S}^{\text{pred}} \quad \text{if } \Phi^{\text{pred}} \leq 0 \text{ (stick)}$$

$$f_{T_S}^{\text{corr}} = \mu f_{N_S}^{\text{cont}} \frac{f_{T_S}^{\text{pred}}}{|f_{T_S}^{\text{pred}}|} \quad \text{if } \Phi^{\text{pred}} > 0 \text{ (slip)}$$

Taking into account the correction of the tangential component of the nodal acceleration for each slave nodes  $\ddot{\mathbf{U}}_{T_S}$  depending on  $f_{T_S}^{\text{corr}}$ , the final corrected acceleration of the slave nodes with friction is calculated as

$$\ddot{\mathbf{U}}_S^{\text{corr}} = \ddot{\mathbf{U}}_S^{\text{pred}} + \ddot{\mathbf{U}}_{N_S} + \ddot{\mathbf{U}}_{T_S}$$

Finally, the vector of contact forces includes both the normal and tangential components, and the updated configuration accounts for the tangential movement of surfaces in contact due to slipping.

An overview of the explicit scheme used for the contact problem stated within the kinematic constraint approach is given in Fig. 5. For the first time step, the internal and external forces are determined based on the initial state. From this information the predictor calculates the accelerations without accounting for the contact constraints given and updates the velocities and displacement to the predicted kinematic state. Then, the algorithm evaluates which nodes are in contact by performing contact searching. The nodes in contact are included into a set of active constraints. These nodes are used by the corrector to apply to them contact forces and to calculate the corrected accelerations. For nodes in contact the vector of contact forces is a sum of the normal and tangential contact forces. The latter components are evaluated according to isotropic Coulomb's law. The slip is tracked by updating the velocities and displacements of nodes satisfying to the slip criterion. The accelerations updated over all nodes are used to calculate the final configuration in which the surfaces in contact are enforced to follow exactly the constraints applied.

1. Initial conditions and initialization;
2. Predictor:
  - Loop over all nodes  $I = 1, \dots$
  - Compute accelerations without accounting for interface interactions  $\ddot{\mathbf{U}}_I^{\text{pred}}$ ;
  - Update velocities and displacements to the predicted configuration:  $\dot{\mathbf{U}}_{i+1/2}^{\text{pred}}$  and  $\mathbf{U}_{i+1}^{\text{pred}}$
  - End loop
3. Check for nodes in contact:  $\mathcal{A}$ 
  - if NO contact go to 5
4. Corrector:
  - Loop over nodes  $S \in \mathcal{A}$
  - Compute contact forces:  $\mathbf{F}_{i+1}^{\text{cont}} = \mathbf{F}_{N_{i+1}}^{\text{cont}} + \mathbf{F}_{T_{i+1}}^{\text{cont}}$
  - Correct accelerations:  $\ddot{\mathbf{U}}_i^{\text{corr}}$
  - End loop
5. Update acceleration over all nodes:  $\ddot{\mathbf{U}}_i$
6. Loop over all nodes  $I = 1, \dots$ 
  - Update the configuration:  $\dot{\mathbf{U}}_{i+1/2}^{\text{pred}}$  and  $\mathbf{U}_{i+1}^{\text{pred}}$
  - Compute stresses and nodal external, internal, damping, hourglass resisting (optionally) forces at  $t_{i+1}$
  - End loop

Fig. 5. Algorithmic setting for the dynamic contact problem within the explicit time-stepping.

The described process continues until the last time step is being reached. ABAQUS/Explicit integrates the set of equations of motion through time very quickly by using many small time increments. The time increment is controlled by the code based on the stability limit. Hence, the time incrementation scheme is fully automatic and requires no user intervention.

#### 4. Numerical results

The free vibration, dynamic transient and dynamic forced analyses of sandwich plates with a circular debonded zone are carried out using the ABAQUS code. One configuration of the sandwich plate is used throughout this study. A simply supported rectangular sandwich plate of 180 mm by 270 mm consisting of a 50 mm-thick WF51 foam core and 2.4 mm-thick GFRP face sheets and containing the penny-shaped debonded zone of a 39.3 mm radius at its center is analyzed. Material properties of the constituent materials are given in Table 1. The dimensions and mechanical parameters of the sandwich plate under consideration are adopted as those in [54].

Natural frequencies of both the intact sandwich plate and the plate with debonding were preliminary extracted using the modal analysis without contact in ABAQUS/Standard. The comparison of the first 10 natural frequencies are presented in Table 2. The essential differences between the frequencies can be seen. Due to the decreasing the stiffness of the plate with debonding its frequencies are considerably lower than those of the intact plate. Along with this, the changes in the order of vibration modes were also observed. The associated mode shapes are not presented here. More detailed studies on the influence of debonding on natural frequencies and associated mode shapes of sandwich plates can be found in [17].

##### 4.1. Transient dynamic analysis

To examine the transient response of the debonded sandwich plate, the simply supported plate is subjected to an impulse concentrated force at the central point of the bottom facesheet. The duration of the applied force is chosen much shorter than the analysis time such that

$$F(t) = \begin{cases} F_0, & 0 \leq t \leq t_* \\ 0, & t > t_* \end{cases}$$

with  $t_* = 1$  ms and  $F_0 = 10$  kN.

Most of the experimental works reported that real structures have critical damping ratios in the range from 0 to 10% with values of 1–5% as the typical range [51]. Because no experimental data concerning the damping phenomenon in the plate under consideration are known, the modal damping ratio is assumed equal to 1% of the critical damping ratio throughout this study. This assumption is used to determine the global damping matrix  $\mathbf{C}$  by specifying the appropriate damping parameters in (15). Herewith, because the stiffness proportional damping drastically decreases the stability limit in the explicit time stepping, the stiffness damping parameter is set equal to zero. While, the mass damping parameter is calculated so that the desirable damping ratio is reached for the given vibration mode. The coefficient of friction is accepted equal to  $\mu = 0.1$  that corresponds to the lower boundary of the range of friction coefficients for plastic–plastic material pairs. A detailed examination of the influence of damping and friction on the dynamics of debonded sandwich plates is behind of this study and it can be a goal of future investigations.

Since the behavior of the detached segments of the sandwich plate is assumed to be studied in detail, several deformed shapes of the debonded region corresponding to its ‘breathing’, i.e. closing, opening and partial closing, when some portions are opened, but others are closed, are shown in Fig. 6 at different moments of time. As one can see, during the oscillations the debonding passes from closed to open status and vice versa in a smooth way, encompassing variety of intermediate configurations. Thus, the assumption that

**Table 1**  
Material properties of the foam-cored sandwich plate.

Components	Elastic constants
Foam core	$E_c = 85$ MPa, $G_c = 30$ MPa, $\rho_c = 52$ kg m <sup>-3</sup>
Face sheet	$E_{xx} = E_{zz} = 19.3$ GPa, $E_{yy} = 3.48$ GPa, $G_{zx} = 7.7$ GPa, $G_{xy} = G_{yz} = 1.65$ GPa, $\rho = 1650$ kg m <sup>-3</sup>

**Table 2**  
Natural frequencies (Hz) of the intact and debonded foam-cored sandwich plates.

Mode	Intact	Debonded
1	1066.2	937.19
2	1584.2	1246.6
3	1771.3	1440.2
4	1906.5	1640.9
5	2192.9	1697.6
6	2245.1	2011.6
7	2636.8	2086.8
8	2699.4	2098.9
9	2822.8	2396.0
10	2825.5	2430.4

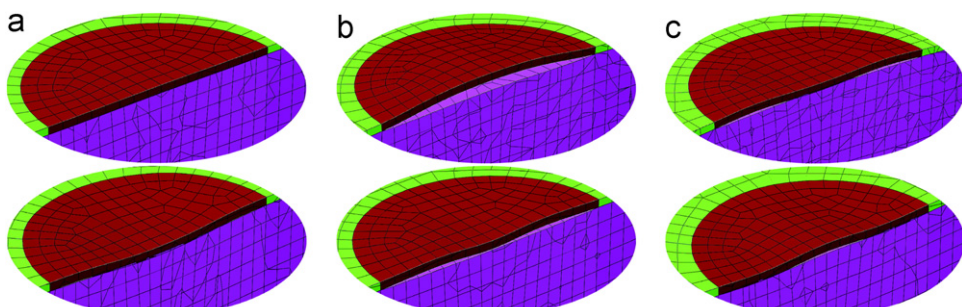


**Fig. 6.** Deformed shapes of the debonded zone: (a) fully closed at  $t = 0.1$  ms and  $t = 1.1$  ms; (b) fully opened at  $t = 0.3$  ms and  $t = 2.2$  ms; and (c) partially closed at  $t = 0.5$  ms and  $t = 5.1$  ms.

the detached segments are either completely open or fully closed, commonly used in the modeling practice, is, in fact, improper and can be considered as an over-simplification of the real behavior. These results are in good accordance with experimental evidences in [22].

It is obvious that when the debonded zone is completely open, stress-free boundary conditions are realized at the damaged interface and no contact forces arise in this region. In the cases of either fully or partially closed debonded zone, the distributed contact forces appear at the local area due to fulfilling of the stress continuity requirements. As mentioned above, the different transition forms between the open and closed statuses in the detached segments occur. Consequently, a variety of contact stress distributions exist. Several such distributions of contact-induced normal stresses on the deformable core target are presented in Fig. 7 at different moments of time. The instants of time at which the stress distributions are presented were chosen so that the more representative contact-induced stress states existing within the debonded zone would be depicted.

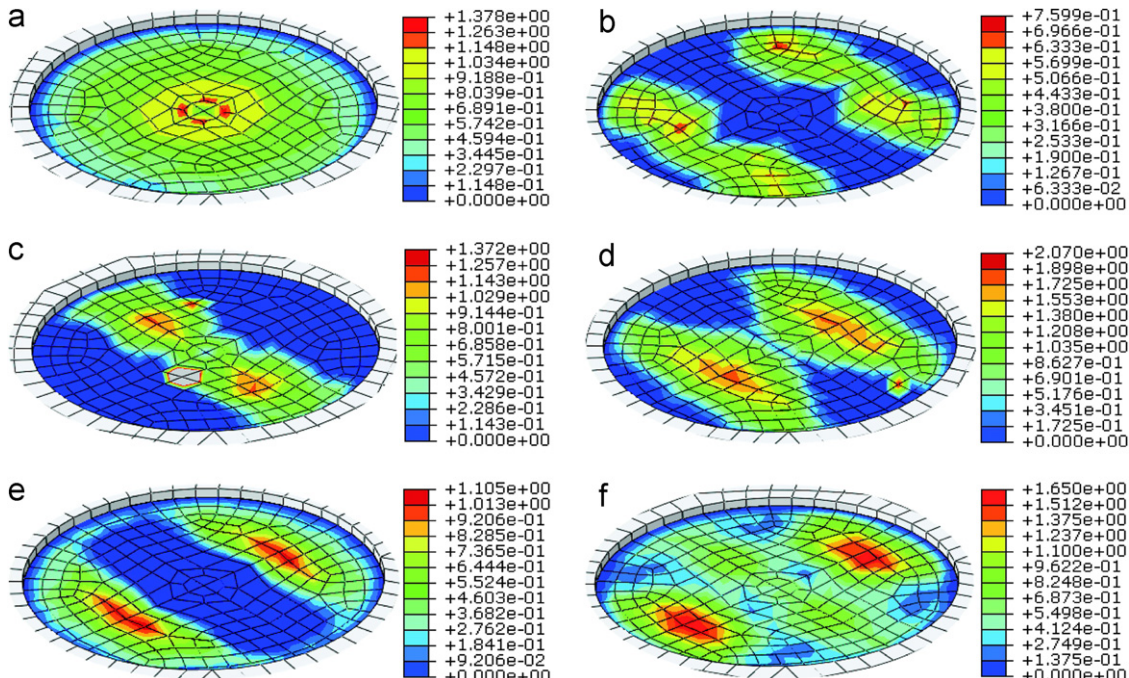
In turn, the contact forces arisen due to the contact behavior between the detached segments contribute to the global dynamic stress state of the sandwich plate. The contour plots of the distributions of Mises stress within the debonded region and a small zone surrounding it at different moments of time for both the intact (on the left hand) and debonded (on the right hand) sandwich plates are compared in Fig. 8. The instants of time are selected in such a way that the differences between the both distributions would clearly be seen.

Fig. 8 shows that the Mises stress in the debonded plate is mainly concentrated within the damaged interface where its level is higher than in the same area of the intact plate. This is caused by both the presence of the boundary of debonded zone, where stresses are concentrated and the contribution of the contact forces within the debonded area. Thus, accurate modeling of the local behavior in the damaged interface is important to understand the global dynamic stress state of the debonded sandwich plate.

Pursuing the aim to find out how the existence of debonding at the facesheet-to-core interface affects the global dynamics of the

sandwich plate, the transient responses of sandwich plates with and without debonding are computed and analyzed further. The comparison of transverse displacements and accelerations calculated at the central point of the upper facesheet (point N 1 in Fig. 3a) for the both plates is shown in Fig. 9. As seen, the presence of the interfacial damage in the sandwich plate significantly changes the transient time histories of displacement and acceleration. The amplitudes of the time histories of the debonded plate are higher than those in the intact sandwich plate. Especially, the biggest difference occurs between the acceleration time histories of the plates, Fig. 9b. Much higher acceleration amplitude of the debonded plate indicates that impact-like contacts between the interacting segments take place. In this kind of motion, when the segments collide each other, the accelerations are the most sensitive means to indicate it. After each hit the magnitude of the acceleration changes in a fast and abrupt way, as shown in Fig. 9b. Similar results were obtained using experimental tests in [21]. Moreover, during the transient motion the debonded sandwich plate oscillates with the longer period of free decay vibrations and with the faster decreasing of vibration amplitudes than those for the intact plate, Fig. 9a. These results are an evidence of the damping effect related to the contact interactions between the detached facesheet and the core. As a result of intermittent contacts additional energy dissipation occurs in the debonded plate.

The fast Fourier transform technique was applied to obtain frequency properties of the both previous transient time histories in Fig. 9. The signals of the response spectrum of amplitudes corresponding to each time-dependent curve in Fig. 9 are illustrated in Fig. 10. By analyzing the displacement curves in the frequency domain in Fig. 10a, two main distinctive features of the signal of the debonded sandwich plate with respect to the signal of the intact sandwich plate can be seen. First, the shift of the fundamental frequency and, second, the appearance of additional peaks before and after the peak of fundamental frequency. The first feature reflects the stiffness reduction due to debonding, whereas the second one evidences the existence of contact interactions between the detached segments. The segments



**Fig. 7.** Distributions of the normal contact stresses within the debonded zone at different moments of time: (a)  $t = 0.1$  ms; (b)  $t = 0.6$  ms; (c)  $t = 1.1$  ms; (d)  $t = 3.0$  ms; (e)  $t = 4.9$  ms; and (f)  $t = 6.0$  ms.

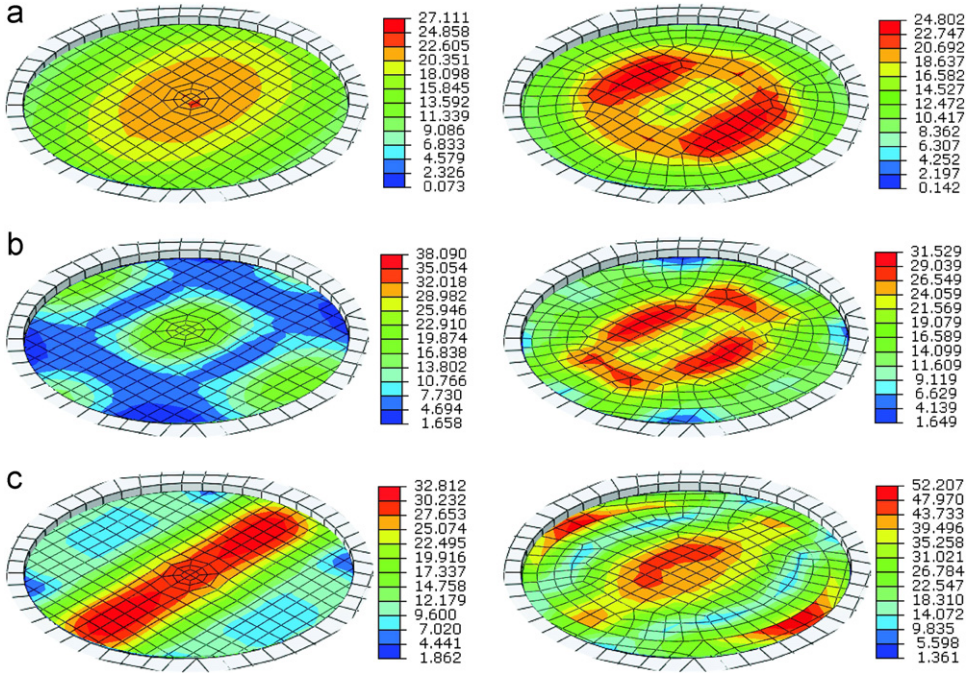


**Fig. 8.** Comparison of the distributions of Mises stress within the debonded zone between the intact (left side) and debonded (right side) sandwich plates at the instants of time: (a)  $t = 0.2$  ms; (b)  $t = 1.1$  ms; and (c)  $t = 2.8$  ms.

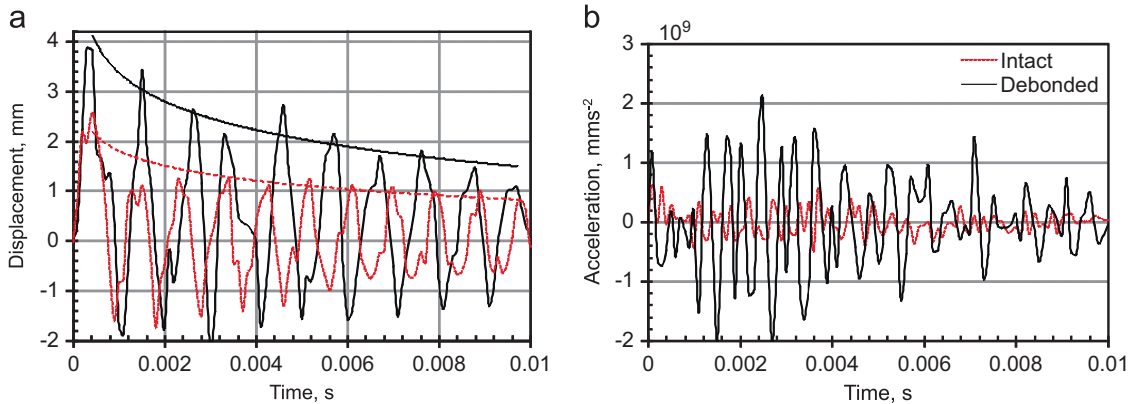


**Fig. 9.** Transient time history outputs at the central point (point N 1 in Fig. 3a): (a) displacement and (b) acceleration.

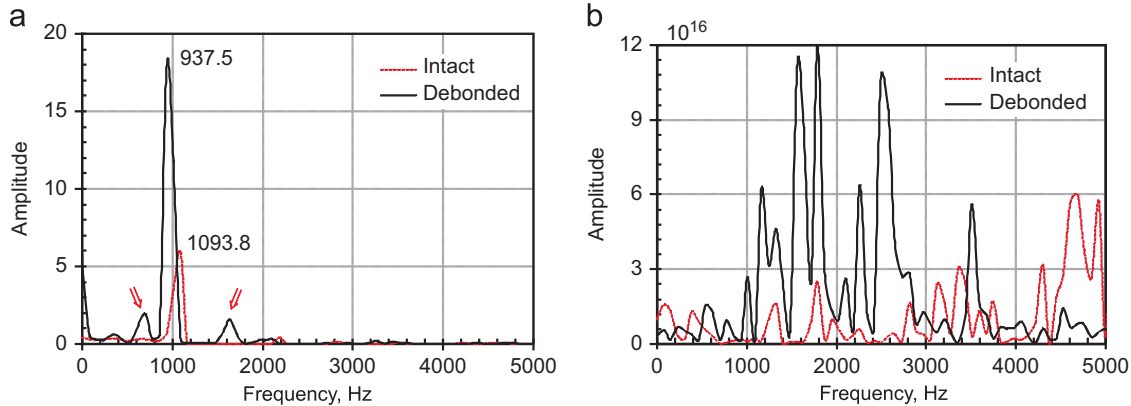


**Fig. 10.** Fast Fourier transforms of (a) the displacement time history and (b) the acceleration time history, calculated at the point N 1 in Fig. 3a.

coming in contact at the local region generate additional frequencies which superpose with the frequency spectrum excited by the external transient load. Also due to local contact the vibration

energy at the fundamental frequency of the debonded plate is greater than that of the intact plate. By comparing the acceleration frequency curves in Fig. 10b, the existence of additional

frequencies in the response spectrum of the debonded plate and changes in the distribution of the vibration energy along the frequency spectrum can be more clearly seen. Besides, Fig. 10b demonstrates that the biggest amplitudes of the vibration energy belong to the frequencies ranged in the middle of the frequency interval, whereas the higher frequencies accumulate the biggest vibration energy in the case of the intact plate. Thereby, the main features of the behavior within the partially debonded interface of real structures such as stiffness reduction, additional inertness and energy dissipation during vibrations that influence on the global dynamics are well simulated with the FE model adopted in this study.

The transient time histories of the Mises stress calculated at the different points of the upper facesheet (points N 1, 2, 3 and 4 in Fig. 3a) of the intact and debonded sandwich plates are compared in Fig. 11. As shown in Fig. 11a and b, the Mises stresses for the both plates at the points of the debonded area (N 1 and N 2) vary with completely different amplitudes. The amplitude of the Mises stress of the debonded plate exceeds the same parameter of the intact plate in several times. While, the amplitudes of the Mises stresses computed at the point far away from the debonded zone (N 3 and N 4) have almost equal values, Fig. 11c and d. Hence, the region of the high level stress within the debonded sandwich plate is confined by the area of the damaged facesheet-to-core interface. But on the other hand this region, where there exist the concentration of the maximum Mises stress, is dangerous to fracture under dynamic loading and debonding propagation is prone to take place at this region. It should be mentioned that the contribution of the contact-induced stresses into the high level of the dynamic stress state within the debonded area was shown earlier as the contour plots of the Mises stress in Fig. 7 and 8.

#### 4.2. Forced dynamic analysis

The forced dynamic analysis of a linear system can be accurately obtained by using the assumption that if the loading is a harmonic function, then the response of the system is also expressed as a harmonic function with the same frequency as the forcing one. However, this assumption is no longer valid for nonlinear systems. Instead of the steady-state analysis, the response of nonlinear systems should be considered within a general dynamic analysis with a loading given by a periodic function [55]. Therefore, to examine the effect of the debonded area on the dynamic response of the sandwich plate when a periodic load is applied, the explicit FE dynamic analysis based on the model described above is carried out further.

The intact and debonded sandwich plates, considered in the previous transient analysis are subjected to a transverse sinusoidal concentrated force with the amplitude of 10 kN applied to the central point of the bottom facesheet. Cases when the driving frequency does not coincide with the fundamental frequency of a system are important from the practical point of view. In this respect, three regimes of forced oscillations are considered in simulations of the sandwich plates. The first two driving frequencies are accepted as fractions of the fundamental frequency such that  $\frac{1}{3}f_1$  and  $\frac{1}{2}f_1$ , and the last forcing frequency is considered as a multiplier of the fundamental frequency  $2f_1$ . Here  $f_1$  denotes the fundamental frequency of the intact plate. Time histories of transverse displacements and velocities calculated at the central point of the top facesheet (point N 1 in Fig. 3a) and phase portraits plotted at the different points N 1, 2 and 3 in Fig. 3a were chosen for presenting the forced dynamics of each of the both plates at the three different frequencies of excitation. The initial displacements and velocities are assumed to be zero. In the forced dynamics a transient motion is

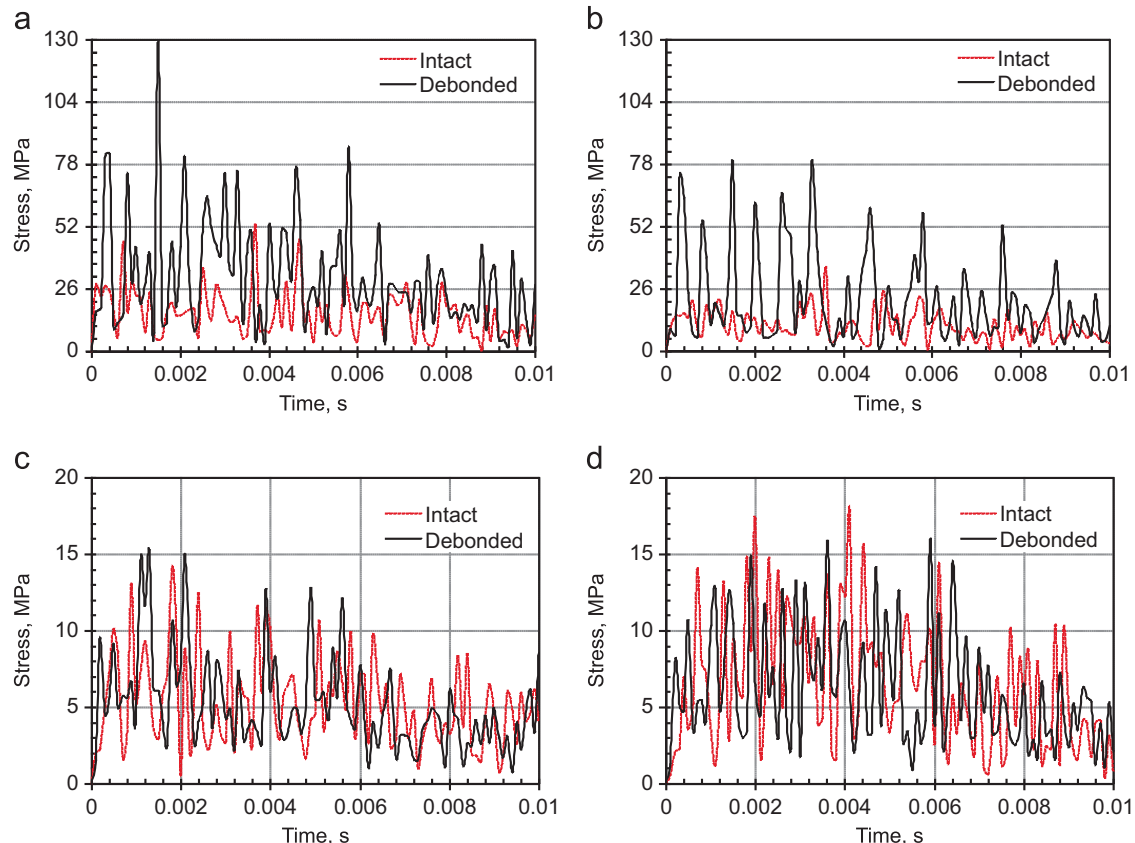
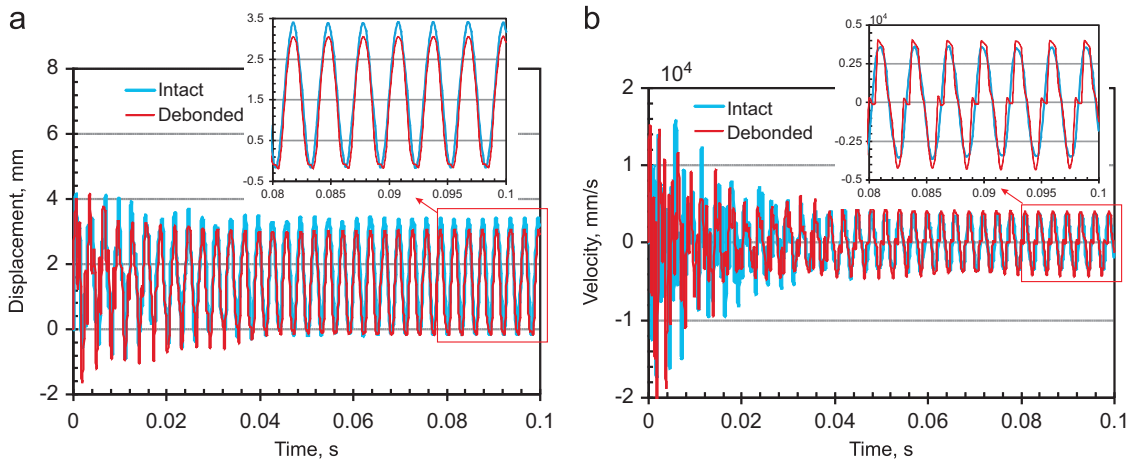


Fig. 11. Transient time history of the Mises stress calculated at the points in Fig. 3a: (a) N 1; (b) N 2; (c) N 3; and (d) N 4.

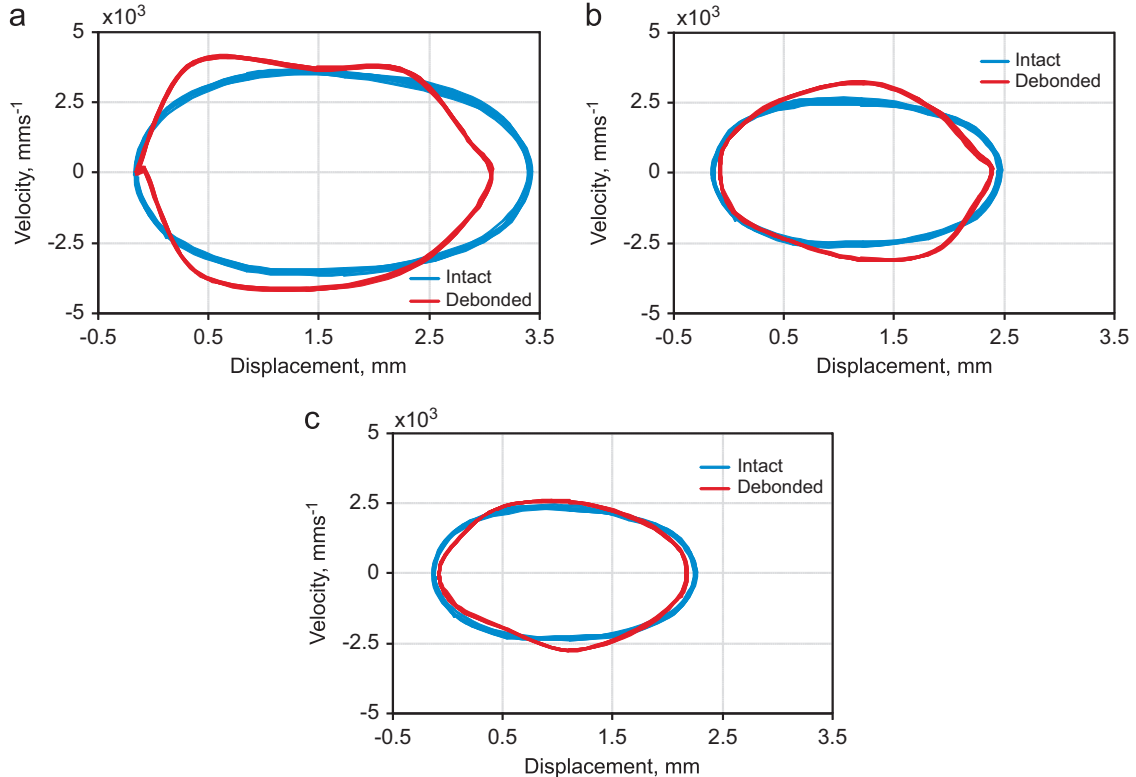
encountered before a steady state motion can be reached. Thus, the analysis time interval was chosen so that the transition to the stationary motion would be observed within a reasonable computational time of calculations. From 3 to 5 h were spent for the simulations presented below. The analysis time interval depends on the type of motion to be computed.

Fig. 12 illustrates time histories of the both plates excited with the driving frequency  $\frac{1}{3}f_1$ . As shown, the displacement and velocity time histories of the intact plate are periodic with a pure sinusoidal waveform that corresponds to its steady-state motion. While, the debonded plate has periodic oscillations with the sinusoidal waveform for the displacement, Fig. 12a, but the waveform of the velocity signal is a little bit modulated, Fig. 12b. The latter fact points out on the existence of a small nonlinearity in a system. In our case it means the presence of

periodic contact between the detached facesheet and the core within the debonded region. In order to investigate this result in more detail, phase portraits of motion at the different points of the upper facesheet surface are shown in Fig. 13. About 20 excitation periods are used for each phase plot. One can see that all phase portraits of the intact plate vibrating harmonically are elliptical. While, the phase curve of the central point of the debonded zone has a form that is significantly disturbed with respect to the elliptical one, Fig. 13a. The phase plots in the points at the boundary of the debonded zone and outside this region show trajectories that are close to elliptical forms, Fig. 13b and c, respectively. Hence, one can conclude that the whole debonded sandwich plate oscillates periodically and harmonically with the forcing frequency, but its local region, where debonding exists, experiences a general periodic motion. This motion is a result of



**Fig. 12.** Time history responses with the exciting frequency  $\frac{1}{3}f_1$  at the central point of the top facesheet: (a) displacement and (b) velocity.



**Fig. 13.** Phase portraits for the exciting frequency  $\frac{1}{3}f_1$  which are calculated at the points in Fig. 3a: (a) N 1; (b) N 2; and (c) N 3.

superposing of the driving frequency and additional harmonics excited by periodic contacts. Thus, at this driving frequency the influence of the local behavior within the debonded region on the global dynamics of the plate is confined by the zone of imperfection only.

When the plates are driven at the frequency of  $\frac{1}{2}f_1$  the response of the intact plate is a steady state motion with the forcing frequency again, but the dynamics of the debonded sandwich plate is much more complicated than in the previous case. As shown in Fig. 14, the signal of the transverse displacement in the debonded plate is a periodic function with a modulated waveform, Fig. 14a, whereas the transverse velocity of this point varies as a quasi-periodic function with a fully

distorted waveform, Fig. 14b. The phase portrait of this point is shown in Fig. 15a. One can see the irregular trajectory with a part resembling an additional loop. Thus, the detached surfaces within the debonded zone are coming into contact in an aperiodic manner as a result of such interactions additional frequencies that may be incommensurate with the driving frequency are generated. One incommensurate frequency (one loop in Fig. 15a) is seen in this case. Furthermore, the quasi-periodic motion at the local debonded zone affects the global dynamics of the whole plate. Fig. 15b and c present the quasi-periodic motion of the plate at the points which are not residing in the debonded zone. Thereby, the quasi-periodic motion is revealed at the driving frequency  $\frac{1}{2}f_1$ .

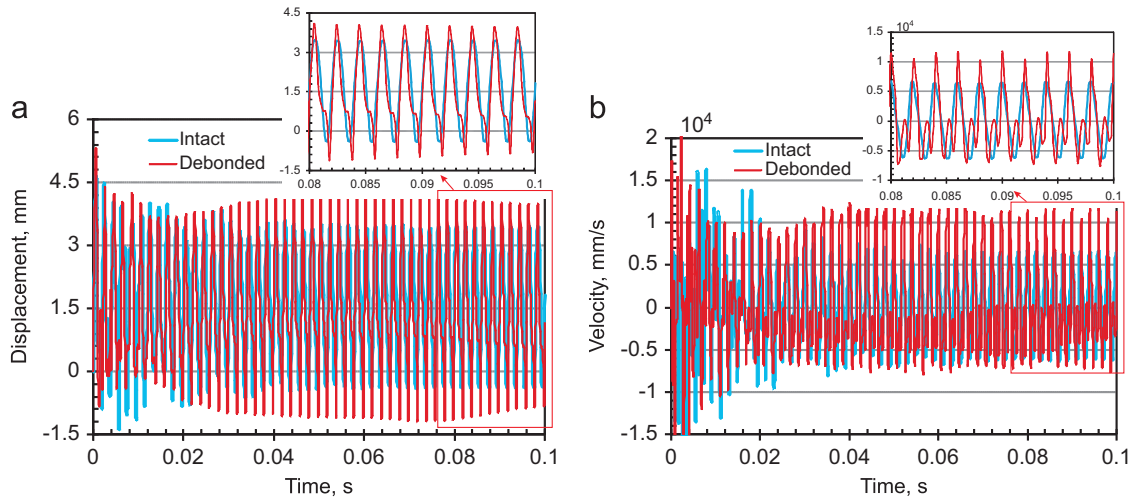


**Fig. 14.** Time history responses with the exciting frequency  $\frac{1}{2}f_1$  at the central point of the top facesheet: (a) displacement and (b) velocity.

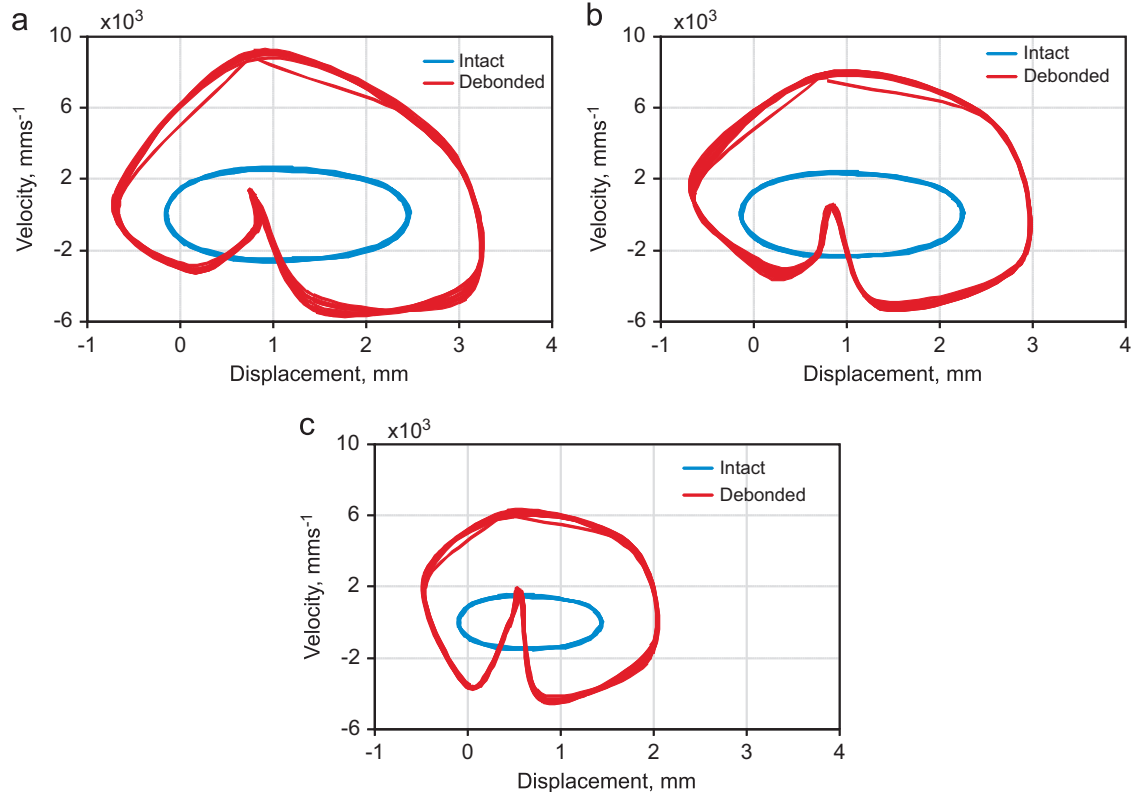


**Fig. 15.** Phase portraits for the exciting frequency  $\frac{1}{2}f_1$  which are calculated at the points in Fig. 3a: (a) N 1; (b) N 2; and (c) N 3.

Finally, at the highest driving frequency  $2f_1$ , which falls down between the 5th and 6th natural frequencies of the debonded plate (Table 2), the dynamics of the debonded sandwich plate differs from the both previous cases of the forced oscillations, Figs. 16 and 17. Comparing the transverse displacements at the central point of the plates with and without debonding, one can see that the signal, extracted from the debonded plate, varies as a quasi-periodic function with large amplitudes and a waveform distorted by the presence of the higher harmonic components, Fig. 16a. However, the velocity time history of this point with respect to the same signal of the intact plate is characterized by the remarkably large amplitudes, considerable distortions of the waveform and losing of the periodicity, Fig. 16b. Such complicated global dynamics of the debonded

sandwich plate results in a conclusion that the detached parts within the plate interact with each other through impact-like irregular contacts. To prove this assertion, phase curves at different points are plotted in Fig. 17. The trajectory of the phase plan at the point N1 is significantly distorted and does not repeat itself exactly, Fig. 17a. Thus, the motion at the central point of the debonded zone is irregular and includes a set of frequencies excited by intermittent contacts. The same conclusion can be drawn for the boundary point of the debonded zone, Fig. 17b. The dynamic behavior of the point far away from the debonding zone reveals a quasi-periodic type of motion, Fig. 17c.

The last two forced analyses can evidence that the application of the steady-state analysis involving the conventional vibration

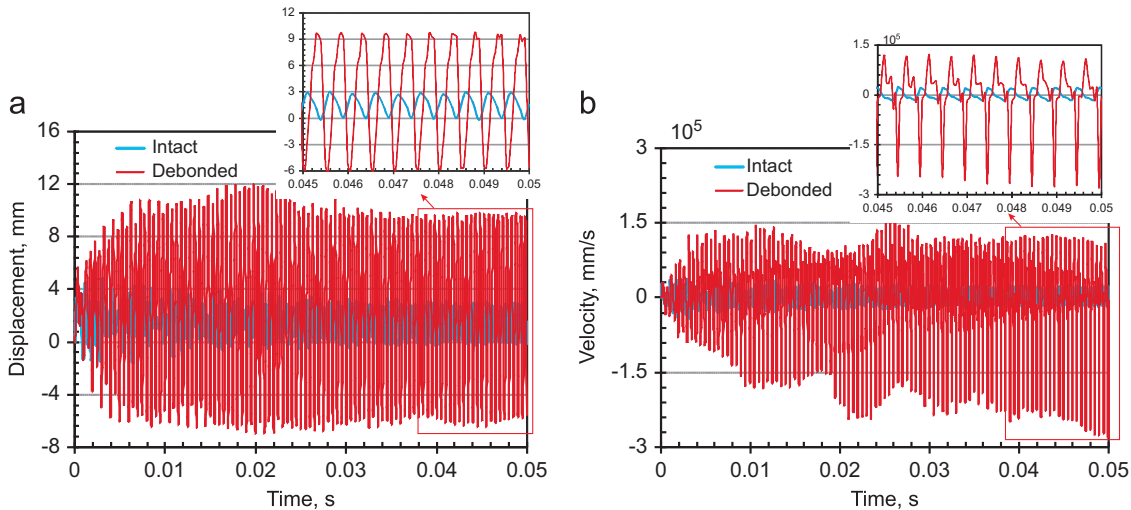


**Fig. 16.** Time history responses with the exciting frequency  $2f_1$  at the central point of the top facesheet: (a) displacement and (b) velocity.

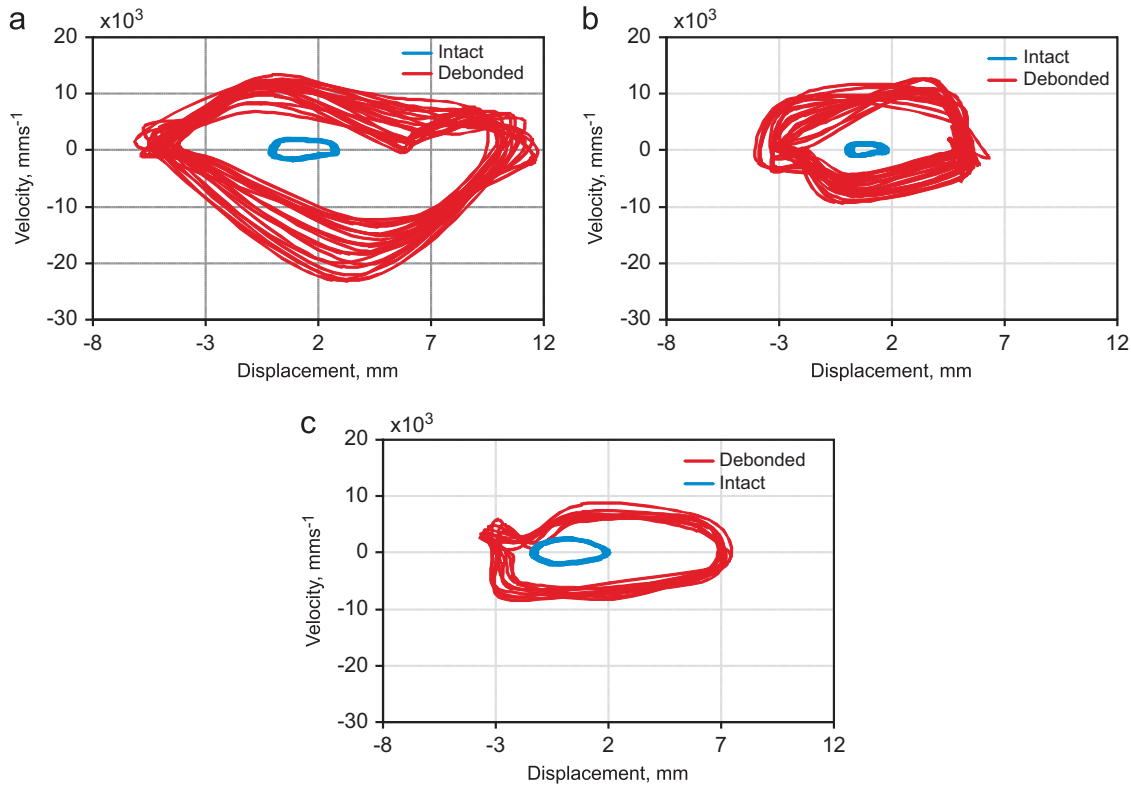


**Fig. 17.** Phase portraits for the exciting frequency  $2f_1$  which are calculated at the points in Fig. 3a: (a) N 1; (b) N 2; and (c) N 3.

techniques based on linear modes would lead to incorrect results for studying dynamic behaviors of debonded plates. The complex interactions between the detached segments at the damaged facesheet-to-core interface result in remarkable changes in the oscillation character of the whole sandwich plate. The higher is a driving frequency, the more indicatively this effect is expressed. These results clearly demonstrate the strongly nonlinear dynamics of the debonded sandwich plate.

## 5. Conclusions

The finite element formulation is applied to study a dynamic behavior of debonded sandwich plates. The three-dimensional finite element model of the sandwich plate with penny-shaped debonded zone located at the plate center has been developed. To gain understanding of the dynamics of this plate, both the transient dynamic analysis under an impulse force and the forced dynamic analysis under a harmonic force were modeled using the ABAQUS/Explicit code. The numerical results showed that both the transient motion and the forced response of the debonded sandwich plate are significantly affected by the presence of the partially detached zone. The transient motion of the debonded plate is accompanied by impact-like contact interactions, which damp the oscillations making them slower and faster decaying than those in the case of the intact plate. Moreover, the local contact behavior changes the frequency properties of the transient signals extracted from the debonded plate in comparing with those for the same intact plate. The debonded plate shows the shift for the fundamental frequency and the presence of several additional frequencies in the response spectrum of amplitudes. It should be mentioned that the intact plate excites predominantly the fundamental mode under such loading. Also, in contrast to the intact plate the magnitude of the frequency response of the debonded plate is significantly higher. Finally, the resulting dynamic stress state in the debonded plate is directly linked to contact stresses arising from the intermittent contact phenomenon. As a consequence, the debonded zone is prone to be the onset of fracture.

Typical features of motion of the debonded plate subjected to a harmonic loading strongly depend on the character of intermittent contacts. This fact is illustrated by analyzing time histories and phase portraits, calculated in the different points of the intact and debonded plates at three different frequencies of excitation. A broad variety of the behavior within the debonded zone such as periodic, quasi-periodic and irregular motions were observed. Besides, it was found that the existence of the quasi-periodicity or the losing of the periodicity in the dynamics of the local imperfect zone resulted in a quasi-periodic motion of the whole sandwich plate.

Finally, from the modeling point of view one can conclude that, first, a steady-state dynamic analysis based on modal approaches is no longer valid for debonded plates, and, second, for an accurate simulation of dynamics of debonded sandwich plates, the contact phenomenon within the debonded region must be taken into account.

## Acknowledgments

This research was performed within the project CEMCAST supported by the 7th Framework Programme, Grant agreement no. 245479 and the project 'Modern material technologies in aerospace industry' of Structural Funds in the Operational Programme - Innovative Economy (OP-IE) financed from the European Regional Development Fund, No. POIG.0101.02-00-015/08

(RT-15: Unconventional technologies of joining elements of aeronautical constructions).

## References

- [1] K.-J. Bathe, *Finite Element Procedures*, Prentice-Hall Inc., New Jersey, 1996.
- [2] L.A. Carlsson, G.A. Kardomateas, *Structural and Failure Mechanics of Sandwich Composites*, Springer Science+Business Media B.V., 2011.
- [3] C.N. Della, D. Shu, Vibration of delaminated composite laminates: a review, *Appl. Mech. Rev.* 60 (2007) 1–20.
- [4] R.L. Ramkumar, S.V. Kulkarni, R.B. Pipes, Free vibration frequencies of a delaminated beam, in: Proceedings of the 34th Annual Technical Conference, Reinforced Plastic/Composite Institute, The Society of the Plastics Industry, 1979.
- [5] J.T.S. Wang, Y.Y. Lin, J.A. Gibby, Vibration of split beams, *J. Sound Vib.* 84 (1982) 491–520.
- [6] P.M. Majumdar, S. Suryanarayn, Flexural vibration of beams with delaminations, *J. Sound Vib.* 125 (1988) 441–4461.
- [7] J.S. Hu, Ch. Hwu, Free vibration of delaminated composite sandwich beams, *AIAA J.* 33 (10) (1995) 1911–1918.
- [8] H.-Y. Kim, W. Hwang, Effect of debonding on natural frequencies and frequency response functions on honeycomb sandwich beams, *Compos. Struct.* 55 (2002) 51–62.
- [9] H. Luo, S. Hanagud, Dynamics of delaminated beams, *Int. J. Solids Struct.* 37 (2000) 1501–1519.
- [10] F. Ju, H.P. Lee, K.H. Lee, Free-vibration analysis of composite beams with multiple delaminations, *Compos. Eng.* 4 (7) (1994) 715–730.
- [11] J. Lee, Free vibration analysis of delaminated composite beams, *Comput. Struct.* 74 (2) (2000) 121–129.
- [12] F. Ju, H.P. Lee, K.H. Lee, Finite element analysis of free vibration of delaminated composite plates, *Compos. Eng.* 5 (2) (1995) 195–209.
- [13] N. Hu, H. Fukunaga, M. Kameyama, Y. Aramaki, F.K. Chang, Vibration analysis of delaminated composite beams and plates using higher-order finite element, *Int. J. Mech. Sci.* 44 (7) (2002) 1479–1503.
- [14] M. Cho, J.-S. Kim, Higher-order zig-zag theory for laminated composites with multiple delaminations, *J. Appl. Mech.* 68 (6) (2001) 869–877.
- [15] S.H. Kim, A. Chattopadhyay, A. Ghoshal, Characterization of delamination effect on composite laminates using a new generalized layerwise approach, *Comput. Struct.* 81 (15) (2003) 1555–1566.
- [16] L.H. Tenek, E.G. Hennekke, M.D. Gunzburger, Vibration of delaminated composite plates and some applications to non-destructive testing, *Compos. Struct.* 23 (1993) 253–262.
- [17] V.N. Burlayenko, T. Sadowski, Influence of skin/core debonding on free vibration behavior of foam and honeycomb cored sandwich plates, *Int. J. Non-Linear Mech.* 45 (10) (2010) 959–968.
- [18] M. Chati, R. Rand, S. Mukherjee, Modal analysis of a cracked beam, *J. Sound Vib.* 207 (2) (1997) 249–270.
- [19] V.V. Matveev, A.P. Bovsunovskii, Some aspects of vibration of an elastic body with a "breathing" discontinuity of material, *Strength Mater.* 32 (5) (2000) 434–445.
- [20] T.G. Chondros, A.D. Dimarogonas, J. Yao, Vibration of a beam with a breathing crack, *J. Sound Vib.* 239 (1) (2001) 57–67.
- [21] P. Vielsack, A vibro-impacting model for the detection of delamination, *J. Sound Vib.* 253 (2) (2002) 347–358.
- [22] I. Müller, A. Konyukhov, P. Vielsack, K. Schweizerhof, Parameter estimation for finite element analyses of stationary oscillations of a vibro-impacting system, *Eng. Struct.* 27 (2005) 191–201.
- [23] X. Lu, W. Lestari, S. Hanagud, Nonlinear vibrations of a delaminated beam, *J. Sound Control* 7 (2001) 803–831.
- [24] A. Saito, B.I. Epureanu, Bilinear modal representations for reduced-order modeling of localized piecewise-linear oscillators, *J. Sound Vib.* 330 (2011) 3442–3457.
- [25] J. Wang, L. Tong, A study of the vibration of delaminated beams using a nonlinear anti-interpenetration constraint model, *Compos. Struct.* 57 (2002) 483–488.
- [26] Y. Fu, Y. Zhang, Nonlinear vibration of beam-plates with a delamination, *Acta Mech. Solidia Sin.* 13 (4) (2000) 353–362.
- [27] H. Schwarts-Givli, O. Rabinovitch, Y. Frostig, High-order nonlinear contact effects in the dynamic behavior of delaminated sandwich panels with a flexible core, *Int. J. Solids Struct.* 44 (2007) 77–99.
- [28] Z.-H. Zhong, *Finite Element Procedures for Contact Impact Problems*, Oxford University Press, Oxford, 1993.
- [29] T.A. Laursen, *Computational Contact and Impact Mechanics: Fundamentals of Modeling Interfacial Phenomena in Nonlinear Finite Element Analysis*, Springer-Verlag, Berlin, 2002.
- [30] P. Wriggers, *Computational Contact Mechanics*, second ed., Springer-Verlag, Berlin, 2006.
- [31] G. Zavarise, P. Wriggers, *Trends in Computational Contact Mechanics*, Springer-Verlag, Berlin, 2011.
- [32] F. Ju, H.P. Lee, K.H. Lee, Dynamic responses of delaminated composite beams with intermittent contact in delaminated segments, *Compos. Eng.* 4 (12) (1994) 1211–1224.

- [33] Y.W. Kwon, H. Aygunes, Dynamic finite element analysis of laminated beams with delamination cracks using contact-impact conditions, *Comput. Struct.* 58 (6) (1996) 1161–1169.
- [34] Y.W. Kwon, D.L. Lannemann, Dynamic numerical modeling and simulation of interfacial cracks in sandwich structures for damage detection, *J. Sandwich Struct. Mater.* 4 (2002) 175–199.
- [35] A. Zak, M. Krawczuk, W. Ostachowicz, Vibration of a laminated composite plate with closing delamination, *J. Intell. Mater. Syst. Struct.* 12 (8) (2001) 545–551.
- [36] A. Ghoshal, H.S. Kim, A. Chattopadhyay, W.H. Prosser, Effect of delamination on transient history of smart composite plates, *Finite Elem. Anal. Des.* 41 (2005) 850–874.
- [37] J. Oh, M. Cho, J.-S. Kim, Dynamic analysis of composite plate with multiple delaminations based on higher-order zigzag theory, *Int. J. Solids Struct.* 42 (2005) 6122–6140.
- [38] V.N. Burlayenko, T. Sadowski, A numerical study of the dynamic response of sandwich plates initially damaged by low velocity impact, *Comput. Mater. Sci.* 52 (1) (2012) 212–216.
- [39] M. Bachene, R. Tiberkak, S. Rechak, Vibration analysis of cracked plates using the extended finite element method, *Arch. Appl. Mech.* 79 (2009) 249–262.
- [40] T. Nagashima, H. Suemasu, X-FEM analyses of a thin-walled composite shell structure with a delamination, *Comput. Struct.* 88 (2010) 549–557.
- [41] J. Dolbow, N. Moës, T. Belytschko, An extended finite element method for modeling crack growth with frictional contact, *Comput. Methods Appl. Mech. Eng.* 190 (2001) 6825–6845.
- [42] J.-H. Song, T. Belytschko, Cracking node method for dynamic fracture with finite elements, *Int. J. Numer. Methods Eng.* 77 (2009) 360–385.
- [43] D. Motamed, S. Mohammadi, Dynamic analysis of fixed cracks in composites by the extended finite element method, *Eng. Fract. Mech.* 77 (2010) 3373–3393.
- [44] I. Harari, J. Dolbow, Analysis of an efficient finite element method for embedded interface problems, *Comput. Mech.* 46 (1) (2010) 205–211.
- [45] ABAQUS User Manual Ver 6.9EF-1, Dassault Systèmes Simulia Corp., Providence, RI, 2009.
- [46] T. Belytschko, W.K. Liu, B. Moran, *Nonlinear Finite Elements for Continua and Structures*, John Wiley and Sons, 2002.
- [47] K. Kikuchi, J.T. Oden, *Contact Problems in Elasticity: A Study of Variational Inequalities and Finite Element Methods*, Society for Industry and Applied Mathematics, Philadelphia, 1988.
- [48] A.L. Eterovic, K.-J. Bathe, On the treatment of inequality constraints arising from contact conditions in finite element analysis, *Comput. Struct.* 40 (2) (1991) 203–209.
- [49] S.A. Meguid, A. Czekanski, Advances in computational contact mechanics, *Int. J. Mech. Mater. Des.* 4 (2008) 419–443.
- [50] A.B. Chaudhary, K.-J. Bathe, A solution method for static and dynamic analysis of three-dimensional contact problems with friction, *Comput. Struct.* 24 (1986) 855–873.
- [51] M. Petyt, *Introduction to Finite Element Vibration Analysis*, second ed., Cambridge University Press, 2010.
- [52] L.M. Taylor, D.P. Flanagan, PRONTO 3D a Three-dimensional Transient Solid Dynamics Program, Sandia National Laboratories, Albuquerque, NM, 1989.
- [53] Y. Frostig, O.T. Thomsen, High-order free vibration of sandwich panels with a flexible core, *Int. J. Solids Struct.* 41 (2004) 1697–1724.
- [54] V. Rizov, A. Shipsha, D. Zenkert, Indentation study of foam core sandwich composite panels, *Compos. Struct.* 69 (2005) 95–102.
- [55] A. Nayfeh, D. Mook, *Nonlinear Oscillations*, John Wiley and Sons, 1979.